

# Functional Importance of a Proteoglycan Co-Receptor in Pathologic Lymphangiogenesis

Scott C. Johns<sup>1,2</sup>, Xin Yin<sup>1,2,3</sup>, Michael Jeltsch<sup>4</sup>, Joseph R. Bishop<sup>5</sup>, Manuela Schuksz<sup>5</sup>, Roland El Ghazal<sup>1,2</sup>, Sarah A. Wilcox-Adelman<sup>6</sup>, Kari Alitalo<sup>7</sup>, and Mark M. Fuster<sup>1,2</sup>

<sup>1</sup>VA San Diego Healthcare System, Medical and Research Sections, La Jolla, CA 92161; <sup>2</sup>Department of Medicine, Division of Pulmonary and Critical Care, University of California San Diego, La Jolla, CA 92037; <sup>3</sup>Marine Drug Research Institute, Huaihai Institute of Technology, Lianyungang 222005, China; <sup>4</sup>Translational Cancer Biology Research Program, Institute of Biomedicine; Biomedicum Helsinki, 00014 University of Helsinki, Finland; <sup>5</sup>Department of Cellular and Molecular Medicine, Glycobiology Research and Training Center, University of California San Diego, La Jolla, CA 92093; <sup>6</sup>Biomatrix Center, New York University, New York, NY 10010, and; <sup>7</sup>Wihuri Research Institute, Translational Cancer Biology Research Program, and Helsinki University Central Hospital; Biomedicum Helsinki, 00014 University of Helsinki, Finland.

S.C.J., and X.Y. are both first authors.



*Running title:* Proteoglycan Co-Receptor for Lymphangiogenesis

Circulation  
Research

## Subject Terms:

Angiogenesis  
Cell Biology/Structural Biology  
Endothelium/Vascular Type/Nitric Oxide  
Vascular Biology  
Vascular Disease

## Address correspondence to:

Dr. Mark M. Fuster  
VA San Diego Healthcare System  
UCSD Department of Medicine  
Division of Pulmonary and Critical Care  
3350 La Jolla Village Drive  
San Diego, CA 92161  
Tel: 858/552-8585 x7347, or 858/699-8935  
FAX: 858/546-1754  
[mfuster@ucsd.edu](mailto:mfuster@ucsd.edu)

In April 2016, the average time from submission to first decision for all original research papers submitted to *Circulation Research* was 15.28 days.

## ABSTRACT

**Rationale:** Lymphatic vessel growth is mediated by major pro-lymphangiogenic factors such as VEGF-C and -D, among other endothelial effectors. Heparan sulfate is a linear polysaccharide expressed on proteoglycan core proteins on cell-membranes and matrix, playing roles in angiogenesis, although little is known regarding any function(s) in lymphatic remodeling in vivo.

**Objective:** To explore the genetic basis and mechanisms whereby heparan sulfate proteoglycans mediate pathologic lymphatic remodeling.

**Methods and Results:** Lymphatic endothelial deficiency in the major heparan sulfate biosynthetic enzyme N-deacetylase/N-sulfotransferase-1 (*Ndst1*; involved in glycan-chain sulfation) was associated with reduced lymphangiogenesis in pathologic models, including spontaneous neoplasia. Mouse mutants demonstrated tumor-associated lymphatic vessels with apoptotic nuclei. Mutant lymphatic endothelia demonstrated impaired mitogen (Erk) and survival (Akt) pathway signaling as well as reduced VEGF-C mediated protection from starvation-induced apoptosis. Lymphatic endothelial specific *Ndst1* deficiency (in *Ndst1<sup>fl/fl</sup>Prox1<sup>+/CreERT2</sup>* mice) was sufficient to inhibit VEGF-C dependent lymphangiogenesis. Lymphatic heparan sulfate deficiency reduced phosphorylation of the major lymphatic growth receptor VEGFR-3 in response to multiple VEGF-C species. Syndecan-4 was the dominantly expressed heparan sulfate proteoglycan in mouse lymphatic endothelia, and pathologic lymphangiogenesis was impaired in *Sdc4(-/-)* mice. On the lymphatic cell surface, VEGF-C induced robust association between syndecan-4 and VEGFR-3 which was sensitive to glycan disruption. Moreover, VEGFR-3 mitogen and survival signaling was reduced in the setting of *Ndst1* or *Sdc4* deficiency.

**Conclusions:** These findings demonstrate the genetic importance of heparan sulfate and the major lymphatic proteoglycan syndecan-4 in pathologic lymphatic remodeling. This may introduce novel future strategies to alter pathologic lymphatic-vascular remodeling.

### Keywords:

Lymphatic capillary, endothelium cell growth, proteoglycans, glycosaminoglycan, vascular endothelial growth factor receptor.

### Non-standard Abbreviations and Acronyms:

CHO – Chinese Hamster Ovary  
EDTA – Ethylenediaminetetraacetic acid  
EGF – Epidermal growth factor  
FGF-2 – Fibroblast growth factor-2  
FGFR – FGF receptor  
HRP – Horseradish peroxidase  
HSPG – Heparan Sulfate Proteoglycan  
LEC – Lymphatic endothelial cells  
LLC – Lewis Lung Carcinoma  
LVD – Lymphatic Vessel Density  
MAP - Mitogen activated protein  
MMTV – Mouse mammary tumor virus

*Ndst* - N-deacetylase/ N-sulfotransferase  
PLA – Proximity Ligation Assay  
PMSF – Phenylmethylsulfonyl fluoride  
PyMT – Polyoma middle T-antigen  
Q-PCR – Quantitative PCR  
RTK – Receptor Tyrosine Kinase  
*Sdc* – Syndecan  
siDS – siRNA Duplex Scrambled control  
VEGF – Vascular endothelial growth factor  
VEGFR-2 – VEGF Receptor-2  
VEGFR-3 – VEGF Receptor-3  
XylT - Xylosyltransferase

## INTRODUCTION

Growth and remodeling of lymphatic vasculature in the tumor microenvironment may be supported by a variety of growth factors that stimulate cognate receptors on host lymphatic vessels<sup>1,2</sup>. The process has been shown to contribute to lymph node metastasis<sup>3-5</sup>. It is also known that a dominant pro-lymphangiogenic growth factor, VEGF-C, is frequently over-expressed in primary carcinomas. Along with a unique role in driving developmental lymphangiogenesis<sup>2,6</sup>, VEGF-C also plays critical roles in tumor lymphangiogenesis along with the stimulatory actions of other tumor vascular growth effectors, such as VEGF-A and FGF-2 as well as cytokines<sup>6,7</sup>.

Heparan sulfate is a linear glycan polymer expressed on a variety of proteoglycans which plays important roles in endothelial growth factor binding in unique pathologic contexts, including tumor angiogenesis<sup>8-10</sup>. Heparan sulfate proteoglycans (HSPGs) secreted into tumor matrix may release growth factors upon the action of tumor heparinase, mobilizing “banks” of pro-angiogenic factors bound to sulfated domains on heparan sulfate in tumor matrix<sup>11,12</sup>. Endothelial-surface proteoglycans may act “*in cis*” in a cell-autonomous manner or “*in trans*” to promote endothelial proliferation in response to growth factors<sup>10,13</sup>. While less is known with respect to lymphatic biology, preliminary work points to a role for heparan sulfate in VEGF-C dependent proliferation of lymphatic endothelial cells (LECs) in culture<sup>14</sup>. However, the genetic importance, mechanisms, and proteins involved *in vivo* remain poorly understood.

We generated lymphangiogenesis models in mice bearing a lymphatic deficiency in the heparan sulfate biosynthetic enzyme N-deacetylase/N-sulfotransferase-1 (*Ndst1*), involved in initiating sulfate modifications of nascent heparan sulfate chains<sup>8</sup>. We demonstrate that lymphangiogenesis is inhibited in models of oil-granuloma induced lymphangiogenesis, wound inflammation, and carcinomas on the *Ndst1*-mutant background, including VEGF-C dependent lymphangiogenesis on a stringent lymphatic-specific *Ndst1*-deficient background. The mutation is associated with defects in lymphatic mitogen and survival signaling, and VEGFR-3 phosphorylation in response to VEGF-C. Using proteoglycan expression analyses, gene-targeted mice, and primary-cell mechanistic analyses, we further highlight syndecan-4 as a major HSPG co-receptor required for VEGF-C mitogen and survival signaling which complexes with VEGFR-3 in a glycan-dependent manner upon VEGF-C exposure.

ONLINE FIRST

## METHODS

### *Cells and cell lines.*

Primary LECs were isolated from mouse mesenteric oil-granuloma/lymphangiomas, as previously described<sup>15</sup>, and tested for LYVE-1/podoplanin expression<sup>14</sup>. For some studies, LECs were purified from lungs of *Ndst1*<sup>fl/fl</sup>*TekCre*<sup>+</sup> mutants<sup>16</sup>. Primary human lung LEC (hLEC; Lonza; previously shown >99% pure at 3<sup>rd</sup> passage by Prox1-staining) were also employed. For Lewis lung carcinoma (LLC) models, retroviruses expressing pLTR-mVEGFC-GFP were used to transduce LLCs (kindly provided by G. Thurston; Regeneron) with full-length VEGF-C (LLC-VC cells)<sup>17</sup>, or GFP-expressing empty vector (LLC-ev) cells as controls. The mouse transformed mesenteric lymphatic endothelial cell line (svLEC)<sup>18</sup> was kindly obtained from Dr S. Alexander (LSU Health Sciences Center).

### *Mice and pathologic lymphatic proliferation models.*

Details on mouse models targeting lymphangiogenesis in *Ndst1* and *Sdc4* mutants, including relevant references, are presented in the expanded Online Supplement.

### *Pathologic tissue processing and analysis.*

Tumor/tissue specimens were formalin-fixed, paraffin-embedded, and H&E stained, with immunostaining details outlined in the Online Supplement.

### *Flow cytometry.*

Lung digests were filtered through 100- $\mu$ m strainers (Fisher), subjected to red-cell lysis (eBioscience), and stained with PE-labeled anti-mouse podoplanin (eBioscience) and APC-labeled anti-mouse LYVE-1 (R&D), with Aqua (Biolegend) viability marker for dead-cell exclusion. Dual PE/APC+ live cells were analyzed by a LSRII (BD) cytometer. The quantity of dual-positive cells as a percentage of total cells was analyzed/plotted, and used in statistical analyses comparing lungs from mutant versus control mice.

### *Quantitative PCR analyses.*

RNA was isolated from primary LECs, reverse transcribed (Superscript III, Invitrogen), amplified using gene-specific primers to each core protein, and quantified (triplicate assays) using the  $2^{-\Delta\Delta C_t}$  method relative to  $\beta$ -actin. Primers included those for mouse HSPGs (Online Table I). For *Ndst*, the same method was used with primers for mouse *Ndst1-Ndst4* isoenzymes<sup>14</sup>.

### *siRNA transfections.*

Primary hLEC at near-confluence were transfected with siRNA targeting heparan sulfate biosynthetic enzymes XylT2 (siXylT2) or *Ndst1* (siNdst1), the HSPG core protein syndecan-4 (siSdc4), or receptors VEGFR-2 (siVEGFR-2) or VEGFR-3 (siVEGFR-3); with scrambled-duplex RNA mock-transfectants (siDS) as controls. Transfections (20nM siRNA) were carried out using Lipofectamine (Invitrogen) following manufacturer recommendations. Transfection complex was added in Opti-Mem (Gibco), and incubated for 6hr, with cell recovery overnight in normal growth medium.

### *VEGF-C species.*

Human recombinant mature VEGF-C was purchased (R&D). Untagged Pro-VEGF-C was expressed from full-length cDNA using a CHO dhfr gene-amplification system<sup>19</sup>. This was predominantly a mixture of unprocessed and partially-processed pro-peptide forms of VEGF-C. Highly expressed clones were identified by the ability of the culture supernatant to sustain growth of VEGFR-3/EpoR Ba/F3 cells<sup>20</sup>. The affinity of Pro-VEGF-C for heparin was used in the capture step from serum-free culture supernatant (salt elution from heparin-sepharose column at 0.48M NaCl, with minor peak at 0.53M). Cation exchange chromatography (pH 6.6) and gel filtration were utilized to increase prep homogeneity. Identity was confirmed by Western blotting. A short-form of VEGF-C consisting of minimum-binding domain

residues A112-L215 was prepared as a strep-II tagged protein in drosophila S2 cells, and purified using streptactin resin. It did not bind to heparin. A mutant form of human VEGF-C (VEGF-C<sub>Cys156Ser</sub> R&D) which binds exclusively to VEGFR-3 was used in some studies.

### ***Immunoblotting.***

Detailed methods for Western blotting of lysates following VEGF-C stimulation of LECs are reported in the Online Supplement.

### ***RTK Phospho Arrays.***

Serum-starved hLEC were stimulated +/- Pro-VEGF-C (1  $\mu$ g/ml) for 15min. Lysates from 6-well plates were collected in 500 $\mu$ L Lysis Buffer (R&D Phospho-RTK Array-assay instructions), and cleared with supernatant used in RTK-assay following manufacturer protocol. After blocking, diluted lysates were incubated with slide-arrays (4°C overnight), washed, and anti-phosphotyrosine HRP-tagged antibody was added (2hr at RT), followed by wash, chemiluminescent development, and digital-imaging densitometry. Further array details, including incorporation of MAPK array following VEGF-C stimulation, are described in the Online Supplement.

### ***VEGFR-3 phosphorylation assays.***

Serum-starved cells were treated with VEGF-C species (1  $\mu$ g/ml), and assayed using a human phospho-VEGFR3 Elisa Kit (R&D). Treated cells were lysed (R&D lysis buffer; 30min, 4°C), spun-down, diluted, added to a pre-coated anti-VEGFR3 plate overnight (4°C), followed by anti-phosphotyrosine-HRP (included in Kit). Biotin-anti-VEGFR3 (Reliatech) labeled with streptavidin-HRP (Vector) was added to detect total VEGFR3. After incubating in substrate solution (R&D), reactions were stopped with 2N sulfuric acid. Plates were assayed at absorbance A450nm, with values corrected against total VEGFR-3.

### ***Proximity ligation assays.***

Chamber slides (Lab-Tek) coated with 50 $\mu$ g/mL PurCol (Advanced Biomatrix), layered with serum-starved hLEC were stimulated with human mature VEGF-C (R&D) for 5min +/-pre-treatment with heparinase in some experiments. Cells were fixed in ice-cold methanol for 10min and blocked (Olink PLA-blocking reagent; 30min at 37°C). Rabbit-anti-human VEGFR-3 (Reliatech) (or for some studies, anti-VEGFR-2; Cell Signaling) and goat-anti-human syndecan-4 (R&D) were then added (2  $\mu$ g/ml) together (in blocking solution overnight; 4°C). Following wash, Rabbit(-) and Goat(+) PLA Probes (Duolink assay; Olink Bioscience) were added (1:10 dilution). In other experiments, rabbit-anti-VEGFR-3 was paired with either mouse-anti-human syndecan-1 (Abcam) or mouse-anti-human syndecan-2 (kind gift from G. David) antibodies. Antibodies were directed against extracellular domains, with manufacturer protocol followed (imaging: 40X objective, RT).

### ***Statistics.***

Mean values (+/-SD) were obtained for LVD or apoptotic-body index for each genotype. For some analyses, means were compared using Student's t-test, with normalization to wildtype (or control) baseline values. Paired t-tests were applied for comparing means of paired values (e.g., for multiple experiments examining western phosphorylation responses pre- versus post-VEGF-C species in siRNA versus control transfected cells; comparisons of change in caspase signal in response to VEGF-C in siRNA versus control transfected cells). For some experiments in which binary-type response data was examined (e.g., TUNEL positivity versus negativity of lymphatic vessels or the presence versus absence of LYVE-1/podoplanin dual-positive cells in flow cytometry analyses of tumor lymphatic endothelial cells) the Wald chi-square statistic was employed. Two-way ANOVA was used in the analyses for experiments in which the significance of any interaction between genotype and biological response to growth factor (e.g., VEGF-C dependent lymphangiogenesis) was examined.

A 2-way ANOVA was also applied to assess for phospho-VEGFR-3 responses to VEGF-C as they depend on siRNA status as well as lymphatic endothelial PLA responses to VEGF-C as they depend on treatment +/- heparinase. SPSS version 19, general linear model function, was used to compute these ANOVAs. A P-value of 0.05 or less was considered significant for all analyses.

## RESULTS

*An endothelial mutation resulting in lymphatic Ndst1 deficiency is associated with reduced pathologic lymphangiogenesis and altered lymphatic signaling.*

We assessed lymphangiogenesis in models of granulomatous inflammation, wound inflammation, and tumor lymphatic remodeling on the *Ndst1<sup>fl/fl</sup>TekCre<sup>+</sup>* mutant background. We first employed an established model of oil-granuloma/lymphangioma induction in the mouse abdomen<sup>15</sup>, wherein plaque-like lesions develop intense proliferation of LYVE-1+ lymphatic endothelium expressing VEGFR-3/Flt-4<sup>15,21</sup>. In this model, while the *Ndst1* mutation exists in all endothelia, lesion-associated LYVE-1+ vessel density in *Ndst1<sup>fl/fl</sup>TekCre<sup>+</sup>* mutants was reduced (Fig.1A), suggesting that lymphatic *Ndst1* deficiency affected pathologic lymphangiogenesis. Wound lymphangiogenesis associated with early skin-wound remodeling was also reduced on the mutant background (Fig.1B). To examine tumor lymphangiogenesis, we crossed mutants with a *MMTV-PyMT* spontaneous mammary tumor strain. Tumors demonstrated reduced lymphatic vessel density (LVD) in *Ndst1<sup>fl/fl</sup>TekCre<sup>+</sup>* mutants (Fig.1C, top left). Tumor expression of VEGF-C was confirmed (Fig.1C, top-right). *TekCre* transgene expression is pan-endothelial, and studies quantifying blood-vascular angiogenesis in the mutants (not shown) revealed a 67% reduction in tumor blood-vascular density relative to wildtype by CD105 staining ( $P<0.001$ ) and 50% reduction by CD31 ( $P<0.01$ ). The unique effect of mutation on LYVE-1+ vessel-density coupled with marked tumor VEGF-C production prompted us to further explore the effect of altered lymphatic heparan sulfate on VEGF-C mediated lymphangiogenesis. As a developmental baseline, LVD in the ear-bud of newborn mice, which is uniquely VEGF-C dependent<sup>2</sup>, was modestly reduced in *Ndst1<sup>fl/fl</sup>TekCre<sup>+</sup>* mutants (Online Fig.1A). While the LVD reduction was significant, this did not result in obvious lymphatic developmental defects such as limb edema or chylous ascites. Knock-down of *Ndst1* in primary lung LECs from non-challenged mutants was confirmed by qPCR (Online Fig.1B).

Lymphatic vessels in tumors from *MMTV-PyMT Ndst1<sup>fl/fl</sup>TekCre<sup>+</sup>* mutants were characterized by a greater percentage of lymphatic-associated TUNEL+ apoptotic bodies (Fig.1C, bottom). In separate primary human cell-based studies, we questioned whether altered heparan sulfate biosynthesis might impair VEGF-C mediated protection of primary human LECs (hLEC) from apoptotic stress, as measured by cellular cleaved caspase levels. In pilot studies, VEGF-C consistently lowered the generation of starvation-induced cleaved caspase by hLEC under several media conditions (Online Fig.1I). XylT2-deficient LECs (siXylT2; characterized by impaired glycan-chain initiation) were insensitive to VEGF-C during starvation (Fig.1D, right bar), while control-transfected hLEC consistently showed reduced apoptosis upon starvation in the presence of VEGF-C (Fig.1D, siDS transfection control, left bar). Consistent with this, VEGF-C dependent Akt phosphorylation in siXylT2-targeted hLEC was reduced relative to control cells (Fig.1E). When stimulated with a VEGF-C ligand that binds exclusively to VEGFR-3 (VEGF-C<sub>Cys156Ser</sub>)<sup>22</sup>, Akt phosphorylation in siXylT2 transfected cells was also blunted (Fig.1E; inset graph). We next examined how siNdst1 targeting might affect Akt phosphorylation in response to VEGF-C<sub>Cys156Ser</sub>: Similar results were found (Fig.1F), implying that VEGFR-3 specific Akt signaling is sensitive to altered glycan sulfation. Moreover, mitogen-activated pathway signaling (phospho-Erk1/2) in response to VEGF-C<sub>Cys156Ser</sub> was also sensitive to hLEC *Ndst1* deficiency (Fig.1G). (It is noteworthy that in preliminary collagen-attachment studies, hLEC attachment and spreading was somewhat slowed in *Ndst1*-deficient cells; data not shown).

*Lymphatic-specific deficiency in the sulfation of heparan sulfate results in altered VEGF-C driven tumor lymphangiogenesis.*

To examine the effect of a lymphatic-exclusive mutation in heparan sulfate, we employed mice bearing a conditional mutation in *Ndst1* driven by tamoxifen-inducible *Cre* under the control of the lymphatic-specific promoter *Prox1* (*Ndst1<sup>fl/fl</sup>Prox1<sup>+/-CreERT2</sup>* mutants). In *Prox1<sup>+/-CreERT2</sup>Rosa26R* reporter studies, inguinal and mediastinal lymph nodes (LNs) showed a relatively high degree of *Cre*-LYVE-1 colocalization (Fig.2A, left), noted also in ear dermal-lymphatics, albeit in a more patchy distribution (Fig.2A, right). With this in mind, we established subcutaneous VEGF-C over-expressing Lewis lung carcinomas (LLC-VC) in the right flank of tamoxifen-induced *Ndst1<sup>fl/fl</sup>Prox1<sup>+/-CreERT2</sup>* mutant and wildtype (*Ndst1<sup>fl/fl</sup>Prox1<sup>-/-CreERT2</sup>*) littermates. LYVE-1 staining showed robust lymphangiogenesis only at the tumor periphery in this model. (F4/80 macrophage staining revealed a diffuse-tumor pattern which decreased toward the tumor periphery, with nearly complete non-overlap of F4/80 with LYVE-1 staining; Online Fig.III). The tumors showed no significant difference in size between mutant and wildtype groups (data not shown). Empty-vector control tumors (LLC-ev) were established in the opposite (left) flank of each mouse. In *Cre*- wildtype mice, LLC-VC tumors showed a significantly higher mean LVD than that of LLC-ev tumors (Fig.2B, graph, left bars), indicating a VEGF-C dependent boost in LVD caused by tumor-associated VEGF-C expression in wildtype mice (compare representative photomicrographs of LYVE-1 immunofluorescence on left of panel set, for *Cre*- animals). On the other hand, among *Cre*+ mutants, LVD was not greater in LLC-VC tumors as compared to that of LLC-ev tumors (Fig.2B right panels and graph, right bars). The findings suggest that the inhibitory effect of lymphatic-targeted *Ndst1* mutation on LVD in this model was specifically associated with VEGF-C mediated lymphatic-vessel growth.

To examine lymphatic proliferation in an orthotopic-tumor setting, LLC-VC cells were intravenously injected into *Ndst1<sup>fl/fl</sup>Prox1<sup>+/-CreERT2</sup>* mutants and *Prox1<sup>-/-CreERT2</sup>* controls. The mean quantity of LYVE-1/podoplanin double-positive LECs (as a percentage of total LECs) from lung digests 7d post-injection was reduced in mutants (Fig.2C), indicating an inhibitory effect of mutation on total LECs purified from LLC-VC tumor-harboring lungs.

*Phosphorylation of VEGFR-3 is sensitive to altered biosynthesis of heparan sulfate in cultured human LECs.*

Preliminary assessments of VEGF-C produced by cultured LLC-VC cells revealed unprocessed VEGF-C in the supernatants and lysates. The quantity of this species relative to post-translationally processed, including mature, VEGF-C species produced by the tumors *in vivo* (which we confirmed by western-blotting) is unknown. Since unprocessed VEGF-C contains heparin-binding propeptide extensions<sup>2, 23</sup>, and since non-mature forms of VEGF-C are variably secreted from tumors<sup>24, 25</sup>, we first screened the degree to which Pro-VEGF-C (a mixture of unprocessed and partially-processed VEGF-C pro-peptides) is able to phosphorylate receptor tyrosine kinase (RTK) receptors, including VEGFR-3, in heparan sulfate deficient- versus control hLECs. (Online Fig.IV highlights the composition of Pro-VEGF-C separated on a silver-stained gel.) Initially, in a highly sensitive RTK phospho-array, inhibition of hLEC heparan sulfate biosynthesis robustly blocked Pro-VEGF-C mediated VEGFR-3 phosphorylation (Fig.3A), as well as VEGFR-2 phosphorylation. While phosphorylation of both receptors appeared to be sensitive to the glycan alteration, the baseline phosphorylation of VEGFR-3 upon ligand stimulation appeared to be markedly greater in this primary cell line, consistent with its lymphatic endothelial identity. Nevertheless, the marked sensitivity of VEGFR-2 phosphorylation to glycan targeting points to an additional role for heparan sulfate in facilitating VEGFR-2 activation in response to VEGF-C, reminiscent of its importance in VEGF-A signaling.<sup>26</sup> The effect of glycan targeting on VEGFR-3 phosphorylation in response to Pro-VEGF-C was also tested in a specific (albeit less sensitive) ELISA-

based phospho-VEGFR-3 assay (Fig.3B), with phosphorylation blockade that resulted from siXylT2 targeting. VEGFR-3 phosphorylation by mature VEGF-C was also significantly reduced in siXylT2-targeted hLEC (Fig.3C). Interestingly, siXylT2-inhibition of glycan-chain biosynthesis also inhibited receptor phosphorylation by a minimum receptor-binding species of VEGF-C (Fig.3D) that excludes basic amino acids in the C-terminus (L216–R227; which may contribute to a weak interaction of mature VEGF-C with heparan sulfate<sup>14</sup>), implying an important cell-autonomous role for the glycan in receptor activation.

*Syndecan-4 is a dominant proteoglycan core protein on lymphatic endothelium with functional significance in pathologic lymphangiogenesis.*

We explored whether a dominant proteoglycan might present heparan sulfate on the lymphatic cell-surface. While LECs were not easily purified from tumors, pathologic primary LECs could be isolated from mesenteric oil-granuloma/lymphangioma lesions<sup>14, 15</sup>, and were examined for the repertoire of HSPG core proteins by qPCR. Syndecan-4 was the dominantly expressed lymphatic cell-surface HSPG (Fig.4A, left graph). Cells did not express CD44v3 proteoglycan, known to be expressed by blood-vascular endothelia<sup>27, 28</sup>, although they did express perlecan, which is secreted into basement membranes, and which has been detected around proliferating and collecting lymphatics<sup>29</sup>. The HSPGs expressed by svLEC, an immortalized mouse mesenteric-lymphatic cell line, showed a similar profile (Online Fig.V). It should be noted that we were able to measure a moderate increase in *Sdc4* expression upon *Ndst1* silencing in this cell line (Fig.4A, upper-right graph); however, the expression of the other syndecans did not change in that setting, with *Sdc4* remaining the dominantly expressed lymphatic HSPG.

With this in mind, we generated oil-granuloma/lymphangioma lesions in syndecan-4 null (*Sdc4*<sup>-/-</sup>) mice, and noted reduced lesion LVD (Fig.4B). Lymphangiogenesis in *Sdc4*<sup>-/-</sup> *Ndst1*<sup>fl/fl</sup> *TekCre*<sup>+</sup> double-mutants examined using this pathologic model was not significantly reduced in comparison to that in *Sdc4*<sup>-/-</sup> *Ndst1*<sup>fl/fl</sup> *TekCre*<sup>-</sup> littermates (data not shown), suggesting that syndecan-4 likely serves as a quantitatively “dominant” functional scaffold for lymphatic cell-surface heparan sulfate, playing a critical role in pathologic lymphatic mitogen responses. We also measured HSPG core-protein expression in non-pathologic LECs purified from the lung (Fig.4C) or LNs (Fig.4D) of wildtype and *Ndst1*<sup>fl/fl</sup> *TekCre*<sup>+</sup> mutants. Syndecan-4 was not only the dominant HSPG, but was disproportionately up-regulated in the setting of *Ndst1* deficiency, indicating that targeting the sulfation of lymphatic heparan sulfate up-regulates major HSPG core-protein expression.

*Syndecan-4 specifically associates with VEGFR-3 in response to VEGF-C in human LECs in a heparan sulfate dependent manner, and mediates VEGF-C dependent signaling.*

We asked whether syndecan-4 might associate with VEGFR-3 (as a possible ternary complex) in hLECs upon VEGF-C stimulation. In human LECs, we previously found that expression of *Sdc2* was somewhat greater than that of *Sdc4*<sup>16</sup>. (As a reference, for primary human dermal microvascular *blood-endothelial* cells, *Sdc4* appears to be the dominantly expressed transmembrane HSPG; Online Fig.VI.) Core protein studies also revealed that the dominant cell-surface HSPGs on hLECs were syndecan-2 and syndecan-4 (as assessed by HSPG core-protein blotting; Online Fig.VII). Nevertheless, proximity ligation analysis (PLA) revealed that resting starved hLEC (i.e., pre-VEGF-C stimulation) are characterized by a significant degree of syndecan-4 –VEGFR3 association at baseline. Exposure to mature VEGF-C strikingly increased syndecan-4 –VEGFR-3 association while syndecan-2 –VEGFR-3 association under identical conditions was minimal (Fig.5A and 5B, left side of graph; “hLEC”). The magnitude of syndecan-1 –VEGFR-3 association (not shown) was comparable to that of syndecan-2 –VEGFR-3, with signals remaining <10% that of baseline syndecan-4 –VEGFR-3 signal. Examination of syndecan-4 –VEGFR-3 PLA in the mouse oil-granuloma derived svLEC line also revealed a marked rise in syndecan-4 –VEGFR-3 association upon VEGF-C exposure (quantified in Fig.5B, right graph; “svLEC”). In separate

experiments examining VEGFR-2, stimulation of hLECs with mature VEGF-C did not lead to engagement of syndecan-4 with VEGFR-2 (Fig.5C; representative panels), suggesting that syndecan-4 serves as a specific co-receptor for VEGFR-3. To further explore mechanism, we found that formation of syndecan-4 –VEGFR-3 complexes upon VEGF-C treatment was sensitive to hLEC pre-treatment with heparanase (Fig.5D), suggesting that lymphatic heparan sulfate is required for stabilizing the proteoglycan-receptor complex upon ligand exposure.

With these findings in mind, we asked whether syndecan-4 deficiency might affect signaling by mature VEGF-C: Phosphorylation of the mitogen-pathway intermediate Erk1/2 was sensitive (Fig.5E; representative immunoblot shown to right). As a receptor-signaling control, Erk1/2 phosphorylation in response to VEGF-C was comparatively sensitive to VEGFR-3 deficiency, and somewhat less sensitive to VEGFR-2 deficiency (Fig.5E, upper-right representative histogram). These Erk1/2 signaling findings further prompted us to employ a commercial phospho-signaling array to examine patterns in VEGF-C dependent activation of other lymphatic endothelial MAP Kinase-associated intermediates in the setting of syndecan-4 silencing. In addition to replicating the pattern we found in Erk phosphorylation in the array (with predominantly Erk1 showing a blunted response to VEGF-C stimulation in the setting of syndecan-4 deficiency), we also noted inhibition of a second MAP Kinase intermediate (p38 $\alpha$ ) along with associated inhibition of HSP27 phosphorylation in the same setting (Fig.5F, with quantified responses below). The array also demonstrated concomitant reduction in VEGF-C dependent Akt2 and TOR activation, which corroborates the original findings in Fig.1 showing altered lymphatic endothelial survival signaling as a result of targeting the glycan chain.

## DISCUSSION

We examine herein the genetic importance of lymphatic heparan sulfate and that of a key proteoglycan core protein in pathologic lymphangiogenesis. Genetic targeting of the glycan impairs pathologic lymphangiogenesis *in vivo* as well as lymphatic mitogen and survival signaling, and phosphorylation of VEGFR-3 in response to VEGF-C. We also demonstrate the genetic importance of syndecan-4 as a key HSPG that scaffolds heparan sulfate on the lymphatic surface, and propose that it functions as a major co-receptor in VEGF-C mediated pathologic lymphangiogenesis.

In *Ndst1<sup>fl/fl</sup>TekCre<sup>+</sup>* mutants, *Ndst1* inactivation under the *Tek*-promoter generates a pan-endothelial mutation, and *Ndst1* expression in LECs purified from mutants was markedly reduced. Lymphatic signaling via VEGF-C/VEGFR-3 appeared to contribute to lymphatic proliferation in both oil-granuloma/lymphangioma models<sup>21</sup> (Fig.1A) as well as transgenic carcinoma (Fig.1C) models. While altering lymphatic *Ndst1* inhibits VEGF-C dependent sprouting and growth signaling *in vivo*, other heparin-binding growth factors such as VEGF-A, FGF-2, or PDGF may also contribute to lymphatic growth and remodeling. Nevertheless, deficiency in the glycan not only altered VEGF-C-mediated protection of primary LECs from apoptotic stress (Fig.1C, bottom); but consistent with this, Erk- and Akt-mediated signaling in primary hLECs was also inhibited in mutants (Fig.1E-G). Pathologic blood-vascular angiogenesis appeared to be altered in such pan-endothelial *Ndst1* mutants, consistent with previous work<sup>10</sup>. While an indirect effect of the blood-vascular mutation on lymphangiogenesis is possible in the setting of pathological angiogenesis, findings employing high-specificity lymphatic gene targeting *in vivo* (discussed below) together with ex-vivo and cell-based work herein point to an important and direct role for lymphatic-specific heparan sulfate in VEGF-C mediated VEGFR-3 activation.

To stringently target heparan sulfate in VEGF-C-mediated lymphatic-specific remodeling, we employed a VEGF-C expressing lung carcinoma model on a genetic background wherein *Ndst1* is specifically inactivated in lymphatic endothelium through the *Prox1<sup>+/CreERT2</sup>* transgene. The findings point to the genetic importance of appropriately sulfated heparan sulfate in mediating the action of VEGF-C on lymphatic endothelium in vivo (Fig.2B). It is possible that non-mature forms of VEGF-C produced by this and/or other neoplastic cell-lines<sup>24</sup> may be more sensitive to the effects of tumor-lymphatic *Ndst1* mutation on VEGFR-3 activation since such species have a greater affinity for heparan sulfate than shorter (e.g., mature) forms of VEGF-C. This may have pathophysiologic importance in neoplasia, where non-mature forms of VEGF-C may play important roles in tumor-lymphatic remodeling, with possibly additional regulation through binding to HSPGs secreted into matrix (e.g., perlecan). It is noteworthy that the predominant species present in Pro-VEGF-C used in Fig.3A,B (i.e., 29/31kD pro-peptide; Online Fig.IV) may compete with other species for VEGFR-3 binding<sup>30</sup>, and thus contribute to negative regulation. This may explain the relatively weak stimulation by Pro-VEGF-C in Fig.3B. Nevertheless, siXylT2 targeting resulted in complete inhibition of VEGFR-3 phosphorylation in this setting, possibly as a result of greater heparan sulfate binding by unprocessed and pro-peptide VEGF-C species. In tumors, this binding may allow for greater presence of pro-peptide VEGF-C on the lymphatic cell-surface, where proteases (e.g., ADAMTS3 tethered to endothelium<sup>30</sup>) may yield local release of mature VEGF-C. Interestingly, VEGFR-3 activation by a non heparin-binding short-form of VEGF-C remained sensitive to altered heparan sulfate biosynthesis (Fig.3D), pointing to the importance of intact lymphatic cell-surface heparan sulfate in VEGFR-3 activation/function. This is reminiscent of altered VEGFR-2 responses to a key non-heparin-binding form of VEGF-A (i.e., VEGF<sub>121</sub>) when endothelial heparan sulfate is genetically altered<sup>26</sup>.

A variety of proteoglycans may tether heparan sulfate to the lymphatic cell-surface or pericellular matrix<sup>8</sup>. While we found abundant expression of syndecan-4 on lymphatic endothelium (Fig.4), a model limitation is that *Sdc4*<sup>-/-</sup> mutation is not tissue-specific. However, pairing the genetic importance of appropriate glycan-sulfation in lymphangiogenesis with the finding that syndecan-4 forms a specific and robust association with VEGFR-3 in response to VEGF-C (Fig.5A-C) suggests that syndecan-4 plays a critical role in VEGFR-3 mediated lymphatic growth. Importantly, the VEGFR-3 specific mitogen response to VEGF-C appears to be glycan-dependent (Fig.5D) and reduced in the setting of syndecan-4 deficiency. In light of the altered signaling with this mutation (Fig.5E), the collective findings suggest that lymphatic-endothelial syndecan-4 deficiency (or *Ndst1* deficiency, which would affect glycans on all HSPGs, including the dominant membrane-bound pool of syndecan-4) results in both altered mitogen-pathway as well as altered survival/Akt signaling (Fig.1F,G as well as Fig.5E). While other HSPGs could theoretically partially “compensate” through the collective actions of their glycans to partially support mitogen-pathway responses in syndecan-4 deficient lymphatic endothelium, the silencing of this unique proteoglycan appears to critically alter lymphatic VEGFR-3 dependent growth/survival signaling and possibly pathways that impact cytoskeletal rearrangement during pathologic lymphangiogenesis. Interestingly, the cooperative activation of Erk1/2 along with p38 MAPK and HSP27 (which we found altered in VEGF-C treated syndecan-4 deficient primary LECs; Fig.5F) has been reported to play an important role in endothelial actin cytoskeletal reorganization in response to VEGF-A, with known inhibition of HSP27 phosphorylation in response to several angiogenesis-pathway inhibitors<sup>31-33</sup>. The findings suggest that VEGF-C mediated activation of this pathway during lymphatic endothelial cytoskeletal remodeling may also be important, and sensitive to alterations in syndecan-4 as a co-receptor. More generally, the findings point to a critical co-receptor role for the dominant lymphatic HSPG syndecan-4 in pathologic lymphangiogenesis.

Figure 6 shows a model to illustrate the functional importance of these molecules in lymphatic receptor functions: In one mode, glycans on the lymphatic surface may serve in a cell-autonomous role as a depot for VEGF-C that in turn may impact availability for VEGFR-3 interactions (Fig.6, pathway B to right). The degree of this may depend on the species of VEGF-C available and the heparin-binding

affinity of that species; with signaling by the different species variably sensitive to genetic absence of the glycan on the cell surface (Fig.3B-D). On the other hand, the glycan appears to play an essential role in stabilizing a ternary complex that mediates proximity of the proteoglycan core protein to the growth receptor (Fig.5), with the HSPG thus serving as a co-receptor (Fig.6, bottom). This may occur either “simultaneously” when ligand becomes available (Fig.6, pathway A), or step-wise via initial concentration and availability of the ligand for receptor-binding events prior to complex stabilization (Fig.6, two-step pathway B). Conceptually, in considering distinct vascular beds, this leaves the possibility of proteoglycan core proteins other than syndecan-4 that could depend on the common glycan (heparan sulfate) in mediating receptor activation in response to VEGF-C. However, in the proof-of-concept studies shown here, we have demonstrated important roles for heparan sulfate expressed on lymphatic endothelial syndecan-4.

These findings may have translational potential. In tumors, while alterations in lymphatic vessel density might not primarily affect primary tumor size, the alteration in lymphatic conduit may reduce the potential for lymphatic metastasis; and in many invasive tumors, up-regulation of VEGF-C as well as the expression of other heparin-binding growth factors and cytokines contributes to tumor lymphangiogenesis<sup>2, 6, 34</sup>. Considering also the roles of both *Ndst1* (appropriate glycan chain sulfation) and syndecan-4 in the proliferation of lymphatic vessels as well as the mechanistic importance of syndecan-4 as a co-receptor for lymphatic signaling (Fig.6, illustration), approaches that target the expression of these molecules in the lymphatic microenvironment may serve as new selective strategies to modulate critical lymphatic remodeling in disease.

#### **ACKNOWLEDGEMENTS**

We appreciate advice and review by Dr. Jeffrey Esko, and histology assistance by Dr. Nissi Varki as well as members of her core-histology team. We acknowledge Dr P. Goetinck for *Sdc4* homozygous-null mice as well as Dr Guillermo Oliver for original provision of *Prox1Cre/ERT2* transgenic mice. We thank Dr Steven Alexander for providing the SV-LEC cell line; and Dr Guido David for 3G10 and Syndecan-2 antibodies. We thank Dr Gavin Thurston for providing LLC-VC and LLC-ev cell lines. Finally we acknowledge Dr Paul Clopton of the VA San Diego Healthcare System and James Proudfoot of the UCSD Clinical and Translational Research Institute for assistance with statistical analyses. We thank Dr. Philip Gordts for valuable insights as well.

#### **SOURCES OF FUNDING**

We acknowledge funding from NIH/NHLBI (R01-HL107652 to MMF; as well as P01-HL57345), the VA Career Development and Merit Review Programs (VA-CDTA Award and VA-Merit I01BX000987-01 to MMF), the American Cancer Society (RSG-08-153-01-CSM to MMF). We also acknowledge NIH/NHLBI (T32 HL098062 to XY and RE), and appreciate support from the Veterans Medical Research Foundation (MMF) as well as the Academy of Finland (decisions 265982 and 273612 to MJ) and the K. Albin Johansson Foundation (to MJ).

#### **DISCLOSURES**

None.

## REFERENCES

1. Lohela M, Bry M, Tammela T and Alitalo K. VEGFs and receptors involved in angiogenesis versus lymphangiogenesis. *Curr Opin Cell Biol.* 2009;21:154-65.
2. Alitalo K, Tammela T and Petrova TV. Lymphangiogenesis in development and human disease. *Nature.* 2005;438:946-53.
3. Achen MG, McColl BK and Stacker SA. Focus on lymphangiogenesis in tumor metastasis. *Cancer Cell.* 2005;7:121-7.
4. Kyzas PA, Geleff S, Batistatou A, Agnantis NJ and Stefanou D. Evidence for lymphangiogenesis and its prognostic implications in head and neck squamous cell carcinoma. *J Pathol.* 2005;206:170-7.
5. Tammela T and Alitalo K. Lymphangiogenesis: Molecular mechanisms and future promise. *Cell.* 2010;140:460-76.
6. Hirakawa S. Regulation of pathological lymphangiogenesis requires factors distinct from those governing physiological lymphangiogenesis. *J Dermatol Sci.* 2011;61:85-93.
7. Karpanen T, Egeblad M, Karkkainen MJ, Kubo H, Yla-Herttuala S, Jaattela M and Alitalo K. Vascular endothelial growth factor C promotes tumor lymphangiogenesis and intralymphatic tumor growth. *Cancer Res.* 2001;61:1786-90.
8. Bishop JR, Schuksz M and Esko JD. Heparan sulphate proteoglycans fine-tune mammalian physiology. *Nature.* 2007;446:1030-7.
9. Iozzo RV and Sanderson RD. Proteoglycans in cancer biology, tumour microenvironment and angiogenesis. *J Cell Mol Med.* 2011;15:1013-31.
10. Fuster MM, Wang L, Castagnola J, Sikora L, Reddi K, Lee PH, Radek KA, Schuksz M, Bishop JR, Gallo RL, Sriramarao P and Esko JD. Genetic alteration of endothelial heparan sulfate selectively inhibits tumor angiogenesis. *J Cell Biol.* 2007;177:539-49.
11. Yang Y, Macleod V, Miao HQ, Theus A, Zhan F, Shaughnessy JD, Jr., Sawyer J, Li JP, Zcharia E, Vlodavsky I and Sanderson RD. Heparanase enhances syndecan-1 shedding: a novel mechanism for stimulation of tumor growth and metastasis. *J Biol Chem.* 2007;282:13326-33.
12. Vlodavsky I and Friedmann Y. Molecular properties and involvement of heparanase in cancer metastasis and angiogenesis. *J Clin Invest.* 2001;108:341-7.
13. Jakobsson L, Kreuger J, Holmborn K, Lundin L, Eriksson I, Kjellen L and Claesson-Welsh L. Heparan sulfate in trans potentiates VEGFR-mediated angiogenesis. *Dev Cell.* 2006;10:625-34.
14. Yin X, Johns SC, Lawrence R, Xu D, Reddi K, Bishop JR, Varner JA and Fuster MM. Lymphatic endothelial heparan sulfate deficiency results in altered growth responses to vascular endothelial growth factor-C (VEGF-C). *J Biol Chem.* 2011;286:14952-62.
15. Mancardi S, Stanta G, Dusetti N, Bestagno M, Jussila L, Zweyer M, Lunazzi G, Dumont D, Alitalo K and Burrone OR. Lymphatic endothelial tumors induced by intraperitoneal injection of incomplete Freund's adjuvant. *Exp Cell Res.* 1999;246:368-75.
16. Yin X, Truty J, Lawrence R, Johns SC, Srinivasan RS, Handel TM and Fuster MM. A critical role for lymphatic endothelial heparan sulfate in lymph node metastasis. *Mol Cancer.* 2010;9:316.
17. Gale NW, Prevo R, Espinosa J, Ferguson DJ, Dominguez MG, Yancopoulos GD, Thurston G and Jackson DG. Normal lymphatic development and function in mice deficient for the lymphatic hyaluronan receptor LYVE-1. *Mol Cell Biol.* 2007;27:595-604.
18. Ando T, Jordan P, Joh T, Wang Y, Jennings MH, Houghton J and Alexander JS. Isolation and characterization of a novel mouse lymphatic endothelial cell line: SV-LEC. *Lymphat Res Biol.* 2005;3:105-15.
19. Kaufman RJ. Selection and coamplification of heterologous genes in mammalian cells. *Methods Enzymol.* 1990;185:537-66.
20. Achen MG, Roufail S, Domagala T, Catimel B, Nice EC, Geleick DM, Murphy R, Scott AM, Caesar C, Makinen T, Alitalo K and Stacker SA. Monoclonal antibodies to vascular endothelial growth factor-D block its interactions with both VEGF receptor-2 and VEGF receptor-3. *Eur J Biochem.* 2000;267:2505-15.

21. Kasten P, Schnoink G, Bergmann A, Papoutsis M, Buttler K, Rossler J, Weich HA and Wilting J. Similarities and differences of human and experimental mouse lymphangiomas. *Dev Dyn.* 2007;236:2952-61.
22. Joukov V, Kumar V, Sorsa T, Arighi E, Weich H, Saksela O and Alitalo K. A recombinant mutant vascular endothelial growth factor-C that has lost vascular endothelial growth factor receptor-2 binding, activation, and vascular permeability activities. *J Biol Chem.* 1998;273:6599-602.
23. McColl BK, Baldwin ME, Roufai S, Freeman C, Moritz RL, Simpson RJ, Alitalo K, Stacker SA and Achen MG. Plasmin activates the lymphangiogenic growth factors VEGF-C and VEGF-D. *J Exp Med.* 2003;198:863-8.
24. Lopez de Cicco R, Watson JC, Bassi DE, Litwin S and Klein-Szanto AJ. Simultaneous expression of furin and vascular endothelial growth factor in human oral tongue squamous cell carcinoma progression. *Clin Cancer Res.* 2004;10:4480-8.
25. Weich HA, Bando H, Brokelmann M, Baumann P, Toi M, Barleon B, Alitalo K, Sipo B and Sleeman J. Quantification of vascular endothelial growth factor-C (VEGF-C) by a novel ELISA. *J Immunol Methods.* 2004;285:145-55.
26. Xu D, Fuster MM, Lawrence R and Esko JD. Heparan sulfate regulates VEGF165- and VEGF121-mediated vascular hyperpermeability. *J Biol Chem.* 2011;286:737-45.
27. Forster-Horvath C, Meszaros L, Raso E, Dome B, Ladanyi A, Morini M, Albini A and Timar J. Expression of CD44v3 protein in human endothelial cells in vitro and in tumoral microvessels in vivo. *Microvasc Res.* 2004;68:110-8.
28. Seiter S, Engel P, Fohr N and Zoller M. Mitigation of delayed-type hypersensitivity reactions by a CD44 variant isoform v3-specific antibody: blockade of leukocyte egress. *J Invest Dermatol.* 1999;113:11-21.
29. Rutkowski JM, Boardman KC and Swartz MA. Characterization of lymphangiogenesis in a model of adult skin regeneration. *Am J Physiol Heart Circ Physiol.* 2006;291:H1402-10.
30. Jeltsch M, Jha SK, Tvorogov D, Anisimov A, Leppanen VM, Holopainen T, Kivela R, Ortega S, Karpanen T and Alitalo K. CCBE1 enhances lymphangiogenesis via A disintegrin and metalloprotease with thrombospondin motifs-3-mediated vascular endothelial growth factor-C activation. *Circulation.* 2014;129:1962-71.
31. Rousseau S, Houle F, Landry J and Huot J. p38 MAP kinase activation by vascular endothelial growth factor mediates actin reorganization and cell migration in human endothelial cells. *Oncogene.* 1997;15:2169-77.
32. Keezer SM, Ivie SE, Krutzsch HC, Tandle A, Libutti SK and Roberts DD. Angiogenesis inhibitors target the endothelial cell cytoskeleton through altered regulation of heat shock protein 27 and cofilin. *Cancer Res.* 2003;63:6405-12.
33. Nguyen A, Chen P and Cai H. Role of CaMKII in hydrogen peroxide activation of ERK1/2, p38 MAPK, HSP27 and actin reorganization in endothelial cells. *FEBS Lett.* 2004;572:307-13.
34. Liersch R and Detmar M. Lymphangiogenesis in development and disease. *Thromb Haemost.* 2007;98:304-10.

## FIGURE LEGENDS

**Figure 1. Pan-endothelial mutation in heparan sulfate biosynthesis results in altered pathologic lymphangiogenesis, lymphatic-vascular apoptosis, and altered VEGF-C signaling.** (A) Oil-granulomas were generated in *Ndst1f/fTekCre+* mutants and *Cre-* littermates to examine lymphangiogenesis in this model. Sprouting of LYVE-1+ vessels (blue) in lesions was examined by immunohistology (Bar=100 $\mu$ m). Mean lymphatic vessel density graphed to right (n=4 mice/genotype; \*P=0.003 for difference). (B) Wound lymphangiogenesis following a full-thickness punch-type skin lesion was examined in *Ndst1f/fTekCre+* mutants and *Cre-* controls. LYVE-1+ lymphatic vessels are shown (arrows) with wound edge (dotted line; “W”) and adjacent epithelial (“Ep”) surface. Mean lymphatic vessels per wound margin for each genotype graphed below (n=4 mutant and 5 wildtype mice; \*P=0.002 for difference; Bar=50  $\mu$ m). (C) Lymphangiogenesis was examined in a spontaneous breast carcinoma model. Tumor sections from mutant and control females show LYVE-1+ vessels in blue (Bar=100  $\mu$ m), with vessel density plotted (n=4 mice/genotype; \*P=0.004 for difference). Tumor VEGF-C was confirmed (upper-right, immunofluorescence with IgG control; Bar=20  $\mu$ m). Lymphatic apoptotic index (quantity of dual TUNEL/LYVE-1+ vessels as a percentage of total LYVE-1+ vessels for each tumor) was examined: Photomicrographs show examples of blue LYVE-1+ vessels with dark TUNEL+ lymphatic nuclei (arrows) in two of the *Cre+* mutant sections. Apoptotic index is graphed to right (\*P<0.001 for difference; n=4 mice/group; left panels Bar=20  $\mu$ m; right panels Bar=100  $\mu$ m). (D) hLEC were tested for reduction in apoptosis as a result of mature VEGF-C exposure following a 6hr starvation period. In response to VEGF-C exposure, the ratio of cleaved- to total caspase-3 was examined by western, and normalized to densitometry for starved control-transfectant cells (“starv baseline”); with assays carried out in triplicate wells for each condition. Graph: response of XylT2 transfected cells (siXylT2; right bar) compared to that of control hLECs transfected with mock/scrambled RNA (siDS; left bar) (\*P=0.02 for difference; avg of 4 experiments). (E) VEGF-C induced phospho-Akt was examined by western in starved siXylT2-transfected vs control hLEC, with phospho/total Akt normalized and plotted relative to value for starved siDS cells (\*P=0.05 for indicated difference in post-stimulation (+) means; avg of 4 experiments; representative blot shown). Inset graph shows response to a human VEGF-C form (VEGF-CCys156Ser) which binds exclusively to VEGFR-3. (F) Effect of siNdst1 targeting on Akt phosphorylation in response to VEGF-CCys156Ser (\*P<0.01 for difference in means; avg 3 experiments). (G) Effect of siNdst1 targeting on Erk1/2 phosphorylation in response to VEGF-CCys156Ser (\*P=0.03 for difference in means; avg of 3 experiments).

**Figure 2. A lymphatic-specific genetic deficiency in the sulfation of heparan sulfate results in altered VEGF-C driven tumor lymphangiogenesis.** Reporter studies in *Prox1+/CreERT2 Rosa26R* mice examined co-localization of Cre (X-gal positive staining) with LYVE-1+ vessels following tamoxifen induction. (A) LNs draining the lung (mediastinum) showed a high degree of co-localization (left panels), and dermal ear lymphatics (right panel) demonstrated patches of co-localization. (B) Lewis lung carcinoma cells that over-express VEGF-C (“LLC-VC”) were used to establish subcutaneous tumors in the right flank of *Ndst1f/f Prox1Cre+/ERT2* (N=4) mutant mice and *Cre-* littermate controls (N=4). Simultaneously, control LLC cells (“LLC-ev”) were injected into the left flank of the same animals to establish VEGF-C negative control tumors. After 10d, tumors were resected, and lymphangiogenesis was examined by LYVE-1 immunofluorescence. Representative images show LYVE-1+ lymphatic endothelia (red) in tumor sections from mutants (right panels) and controls (left panels). Graph shows mean density of LYVE-1+ lymphatic vessels (+/- SD) in LLC-VC and LLC-ev tumors from *Ndst1f/f Prox1Cre+/ERT2* mutant vs *Cre-* control littermates (\*P = 0.05 for the interaction of genotype with VC versus ev tumor status). In the mutant group, the difference in means was not significant. (C) To examine tumor VEGF-C driven lymphatic proliferation in the lung, LLC-VC cells were intravenously injected into *Ndst1f/f Prox1Cre+/ERT2* mutants (N=5) and *Cre-* (N=5) controls. Mice were euthanized 7d following injection: Tumor-containing lungs from each mouse were digested into a single-cell suspension, and LYVE-1+/podoplanin+ (double-positive) LECs present in the digests were measured by flow cytometry.

Representative panels are shown for *Cre*<sup>+</sup> mutant and *Cre*<sup>-</sup> control mice; and averages (+/-SD) for both groups, expressed as %total cells, are shown in graph to right (\*P <0.001 for the difference with wildtype).

**Figure 3. Disruption of lymphatic heparan sulfate biosynthesis in primary human lymphatic endothelial cells results in reduced phosphorylation of VEGFR-3 in response to distinct VEGF-C species.** A receptor screening format was used to assess how targeting heparan sulfate biosynthesis might alter VEGFR-3 activation in response to distinct VEGF-C species. (A) In a preliminary multiple-receptor screen, cultured serum-starved hLEC transfected with either control/ scrambled RNA (siDS) or siXylT2 were stimulated with Pro-VEGF-C, and phosphorylation of growth receptors from post-stimulation (versus un-stimulated) cell lysates was measured using a receptor tyrosine kinase (RTK) phospho-array, which reports receptor phosphorylation (pair of dots) for all receptors captured from cell-lysate samples. The array for starved control (mock-transfected) hLEC shows a weak phospho-VEGFR-3 signal (upper left slide; dot-pair within box, with arrows also pointing to phospho-VEGFR-2 for reference). The array for control cells 15 min post-stimulation with Pro-VEGF-C (“siDS+ Pro-VEGF-C”) is shown in the lower-left slide. Slides to the right show responses for baseline- versus stimulated siXylT2 transfected hLEC (Dot pairs on corners of each slide are phosphotyrosine positive controls.) Auto-phosphorylation occurred for a few other receptors at baseline, without a major response to Pro-VEGF-C: Those were Flt3 (dot-pair immediately above VEGFR-3), VEGFR-1 (to left of VEGFR-2), Tie-2 (lower-left), HGFR (immediately above/to right of Tie-2), and faintly visible EGFR (upper-left). Signal values normalized to that of starved-control unstimulated cells are plotted on graph to right. A separate array repeated under identical conditions showed similar results. (B) The ability of Pro-VEGF-C to phosphorylate VEGFR-3 in control- (siDS) or siXylT2-transfected hLEC was then exclusively carried out in a capture-ELISA format. Mean signal values normalized to that of control unstimulated cells (siDS, no VEGF-C) are plotted (\*P=0.006 for interaction of siRNA status with VEGF-C stimulation response; average of 3 experiments). (C) The same ELISA-based assay was used to examine the effects of hLEC XylT2 silencing on VEGFR-3 phosphorylation in response to stimulation with human mature VEGF-C, with control-normalized signal values plotted on the graph (\*P=0.006 for the interaction; average of 6 experiments). (D) Responses were examined for stimulation by a short-form of VEGF-C (T103-L216) that does not bind heparin, and contains the minimal receptor-binding domain A112-L215 (\*P=0.01 for the interaction; average of 5 experiments).

**Figure 4. Syndecan 4 is a dominant heparan sulfate proteoglycan in primary lymphatic endothelia, and genetic targeting of syndecan-4 results in altered pathologic lymphangiogenesis.** The genetic importance of proteoglycan core-protein targeting was examined in pathologic lymphangiogenesis. (A) The repertoire of HSPG core proteins expressed by proliferating LECs isolated from oil-granuloma lesions in mice was assessed by quantitative PCR. RNA was isolated, reverse transcribed, amplified using gene specific primers to each core protein, and quantified relative to expression of  $\beta$ -actin. Ct values from triplicate assays were used to calculate % expression. Given the unique expression profile of syndecans, with syndecan-4 as a dominantly-expressed HSPG, expression of the syndecan members was examined in the svLEC mesenteric LEC cell-line in the setting of silencing of *Ndst1* (si*Ndst1*), with comparison to expression by control svLECs, transfected with random (scrambled-duplex) RNA (siDS); with values in graph to upper right. (B) Oil-granuloma lesions were induced in syndecan-4 knockout (*sdc4*<sup>-/-</sup>) mice and wildtype controls. H&E stained sections of the lesions (left) were characterized by dense granuloma cell infiltrates (“Gr”) surrounding oil droplets (“O”), with lesions abutting the abdominal diaphragmatic (“D”) surface. Immuno-staining for LYVE-1 revealed marked lesion-associated lymphangiogenesis in sections from wildtype mice, with lymphatic vessels (arrows, right photomicrographs; Bar=100 $\mu$ m) shown in blue. Mean lymphatic vessel densities are graphed to the right (n=4 mice per genotype; \*P=0.002 for difference). (C) To assess the repertoire of proteoglycan core proteins expressed by other primary non-pathologic LECs purified from the mouse as well as the effect of *Ndst1* mutation on core protein

expression, primary LECs were isolated from the lungs of *Ndst1/fTekCre+* mutants and *Cre-* littermates. RNA from purified LECs was processed (as in **B**) for quantitative PCR, and the expression of major HSPGs was quantified relative to that of  $\beta$ -actin (graph). Expression of the dominant core protein, again noted to be syndecan-4, appeared to be markedly up-regulated in *Ndst1* deficient LECs (light bars in graph). **(D)** Expression was also examined using the same method for primary LECs isolated from the LNs of wildtype and *Ndst1/fTekCre+* mutants, with similar findings.

**Figure 5. Proteoglycan-dependent signaling and complexing of syndecan-4 with VEGFR-3 upon VEGF-C stimulation.** **(A)** Dynamic association of VEGFR-3 with two highly expressed HSPGs (syndecan-2 and -4) on the lymphatic cell-surface was tested in response to mature VEGF-C on serum-starved hLECs via proximity ligation assay (PLA). Proximity of syndecan-4 to VEGFR-3 is shown at baseline (lower right panel; PLA signal, red dots), and following stimulation with mature VEGF-C (upper right; Dapi-nuclei in blue; Bar=50 $\mu$ m). Panels on left show PLA for syndecan-2 and VEGFR-3. **(B)** Split-graph on left shows mean PLA signals for hLECs from multiple experiments (n=3 for syndecan-2 and n=5 for syndecan-4; +/- SEM), normalized to mean for syndecan-4/VEGFR-3 association at baseline (\*\*P=0.03 for difference between baseline and +VEGF-C means). Split-graph to right shows mean syndecan-4/VEGFR-3 PLA signals for mouse svLECs (n=4 experiments; +/- SEM), normalized to baseline (no VEGF-C) (\*\*P=0.03 for difference between baseline and +VEGF-C means). **(C)** PLA to examine syndecan-4/VEGFR-2 association was carried out +/-VEGF-C: representative photomicrographs shown. **(D)** To examine the importance of heparan sulfate, PLA signals in hLECs treated +/- heparinase (destroys heparan sulfate chains) were quantified, normalized to baseline for syndecan-4/VEGFR-3, and graphed (\*P=0.02 for interaction of +/- heparinase status with VEGF-C stimulation response; average of 5 experiments). **(E)** The effect of siRNA targeting of *Sdc4* (siSdc4) on Erk phosphorylation in response to mature VEGF-C was examined in cultured hLEC (\*P=0.04 for difference; average of 4 experiments; representative blot at lower-right). Upper-right inset graph shows representative histogram of effect of siRNA targeting of VEGFR-3 or VEGFR-2 on Erk phosphorylation in the same cells as a mitogen-receptor signaling control. **(F)** Lysates from control (siDS) or siSdc4 hLECs pre/post VEGF-C stimulation were applied to a phospho-signaling array reporting phosphorylation of several MAPK and survival-signaling intermediates (as dot-pairs) on the membranes. Arrays for control cells (siDS) pre/post VEGF-C are shown to left. Slides to right show corresponding signals for siSdc4-transfected hLEC. A box is placed around P-Erk1 for reference, showing marked stimulation in control hLEC with blunted response in syndecan-4 deficient cells, resembling western pattern in **(D)**. Other notable blunted VEGF-C responses in *Sdc4*-deficient cells (graphed below) included p38 $\beta$  (black arrow), survival pathway intermediates (Akt2, TOR; red arrows); and the heat-shock protein HSP27 (arrowhead).

**Figure 6. Schematic showing functions of the lymphatic endothelial heparan sulfate proteoglycan syndecan-4 at the cell surface upon ligand stimulation by VEGF-C.** In one pathway **(A)** introduction of VEGF-C induces association between the growth factor (VEGF-C), proteoglycan (syndecan-4), and receptor (VEGFR-3), wherein the proximity of syndecan-4 to the receptor as well as binding of the ligand is stabilized by the glycan chain. This co-receptor function is necessary for efficient receptor phosphorylation and activation, leading to mitogen-activated cell growth and survival signaling. Absence of the proteoglycan, or lack of an appropriately sulfated glycan chain, is associated with impaired lymphatic growth signaling in response to VEGF-C. An alternative pathway **(B)** highlighting cell-autonomous “ligand-depot” functions of lymphatic endothelial heparan sulfate illustrates the ability of the appropriately sulfated glycan chain to bind VEGF-C, making it available for receptor binding via VEGFR-3 receptors on the cell surface. This may eventually lead to further syndecan-4 – VEGFR-3 proximity and ternary complex formation (bottom).

The “depot” function of heparan sulfate for species of VEGF-C with greater heparin-binding affinity (i.e., pre-proteolytically processed VEGF-C > mature VEGF-C) may be particularly important in regulating availability of those species for interaction with receptor at the cell surface. Regardless, the glycan chain ultimately is necessary to stabilize a proteoglycan co-receptor complex that optimizes cell signaling (bottom, via pathway **B**).



# Circulation Research

---

ONLINE FIRST

## Novelty and Significance

### *What Is Known?*

- Lymphatic vascular remodeling in disease states such as neoplasia or inflammation may facilitate important downstream pathophysiologic events such as lymphatic metastasis or organ fibrosis, among other consequences depending on the tissue and disease process.
- While the major lymphatic vascular mitogen VEGF-C is critical in driving pathologic lymphangiogenesis primarily through the activation of the major lymphatic receptor VEGFR-3, co-receptors that critically regulate ligand and receptor activation are poorly understood.
- Cell-surface proteoglycans displaying sulfated carbohydrate chains known as heparan sulfate are known to play key roles in endothelial growth factor binding and receptor signaling, although the genetic importance and function(s) of these molecules in lymphatic remodeling in vivo remain unknown.



### *What New Information Does This Article Contribute?*

- The sulfation of heparan sulfate on lymphatic endothelium is important in mediating the actions of VEGF-C on lymphatic endothelial growth in pathologic models in vivo.
- Syndecan-4 is a major heparan sulfate proteoglycan expressed on lymphatic endothelium, and serves as a novel coreceptor for lymphatic VEGFR3 signaling, forming a glycan-dependent complex with ligand and receptor upon VEGF-C stimulation.
- Syndecan-4 deficiency results in reduced pathologic lymphangiogenesis and reduced VEGFR-3 mitogen signaling in primary lymphatic endothelial cells, introducing a novel mode of biological modulation and possibly therapeutic targeting.

The process of lymphangiogenesis plays critical roles in the pathologic progression of several important diseases. These include metastasis-promoting lymphatic remodeling in cancer, lymphatic proliferation associated with lymphangiomyomatosis (LAM), or fibrotic progression in idiopathic fibrosis (IPF) and renal tubulointerstitial disease, among others. Overexpression of VEGF-C in the lymphatic microenvironment of these disorders is a central requirement, and growth signaling primarily through the cognate lymphatic VEGFR-3 receptor plays a critical molecular role. We report the genetic importance of a novel glycan co-receptor for pathologic VEGF-C dependent lymphangiogenesis in vivo. Mechanistic work points to important roles for appropriately sulfated lymphatic heparan sulfate in mediating Akt and Erk dependent lymphatic signaling as well as activation of lymphatic endothelial VEGFR-3 by multiple VEGF-C species. We also discovered that syndecan-4 is the major lymphatic heparan sulfate proteoglycan involved in mediating lymphatic VEGF-C – VEGFR-3 complex formation and signaling in a manner that critically depends on its glycan chains, and we propose a novel role for heparan sulfate proteoglycans in mediating this biological process. The findings may guide development of novel glycan-biosynthesis inhibitors or proteoglycan-targeting strategies to inhibit carcinoma spread, fibrosis in a variety of inflammatory states, or conditions where lymphangiogenesis contributes to pathologic progression.

Figure 1

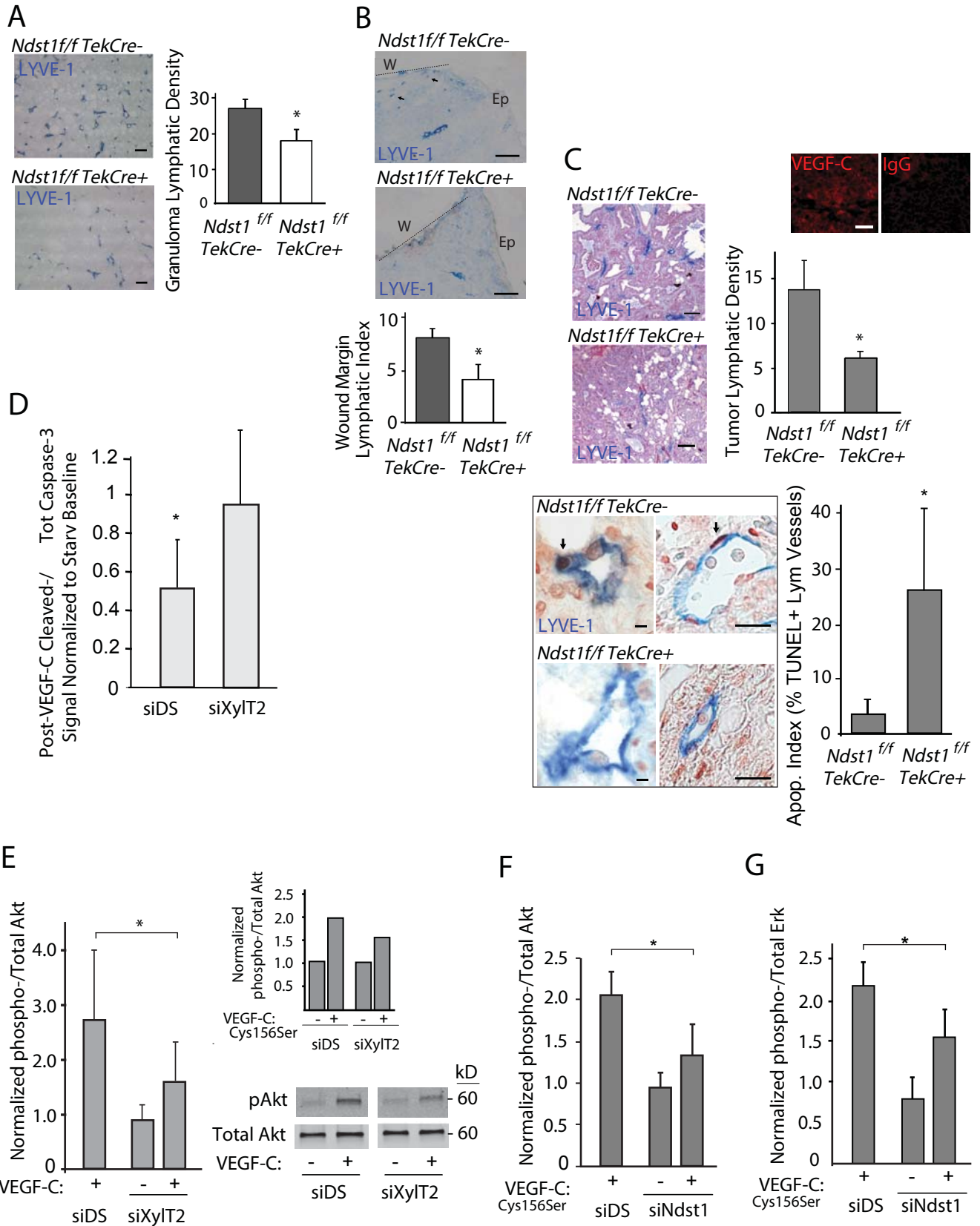


Figure 2

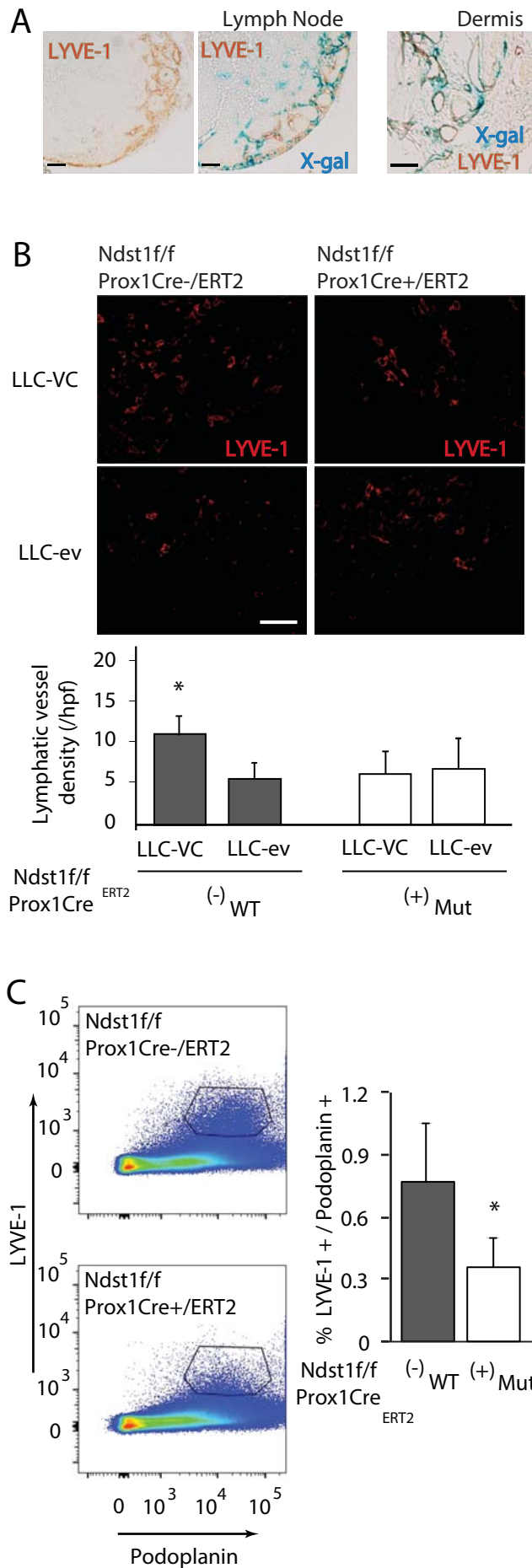


Figure 3

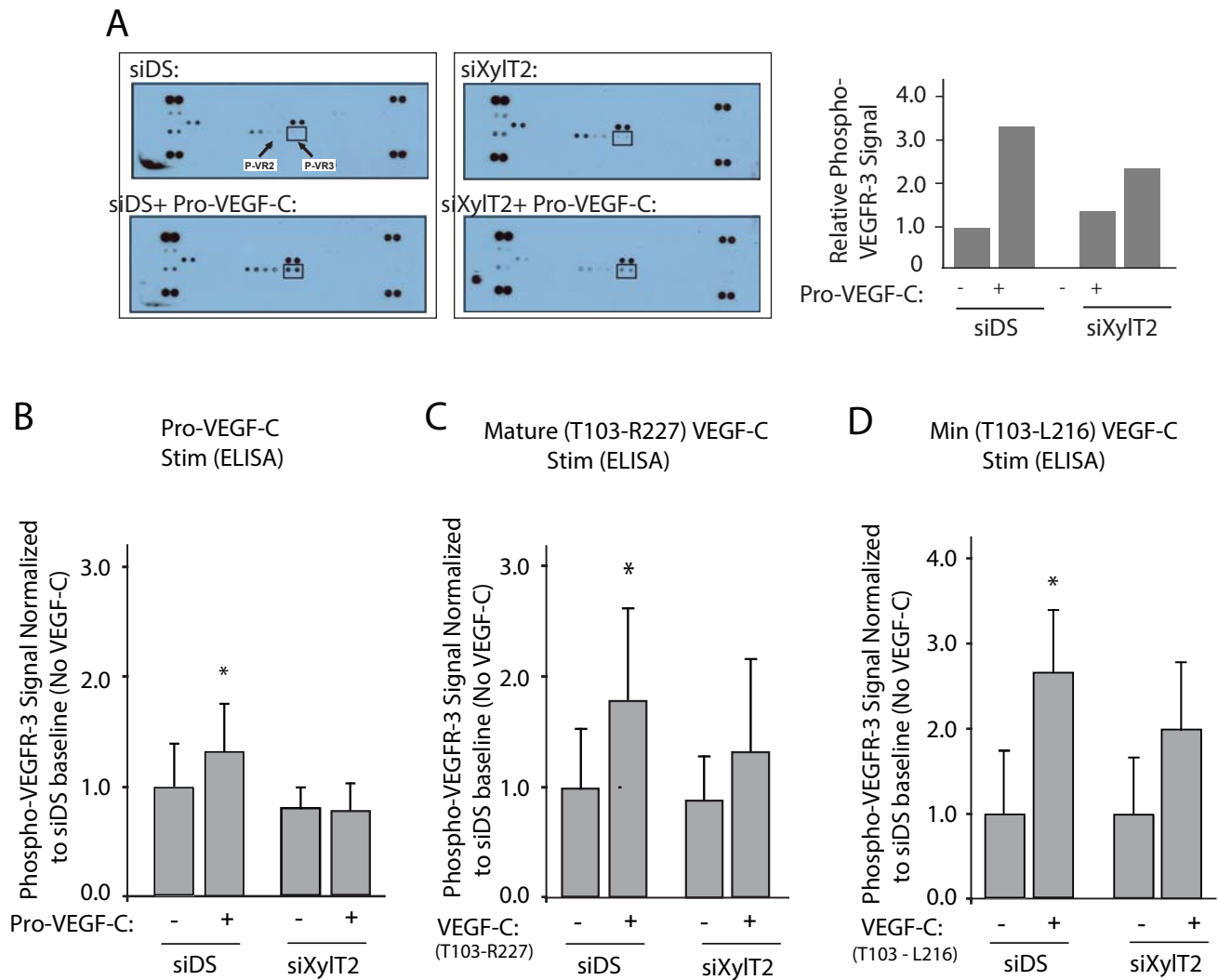


Figure 4

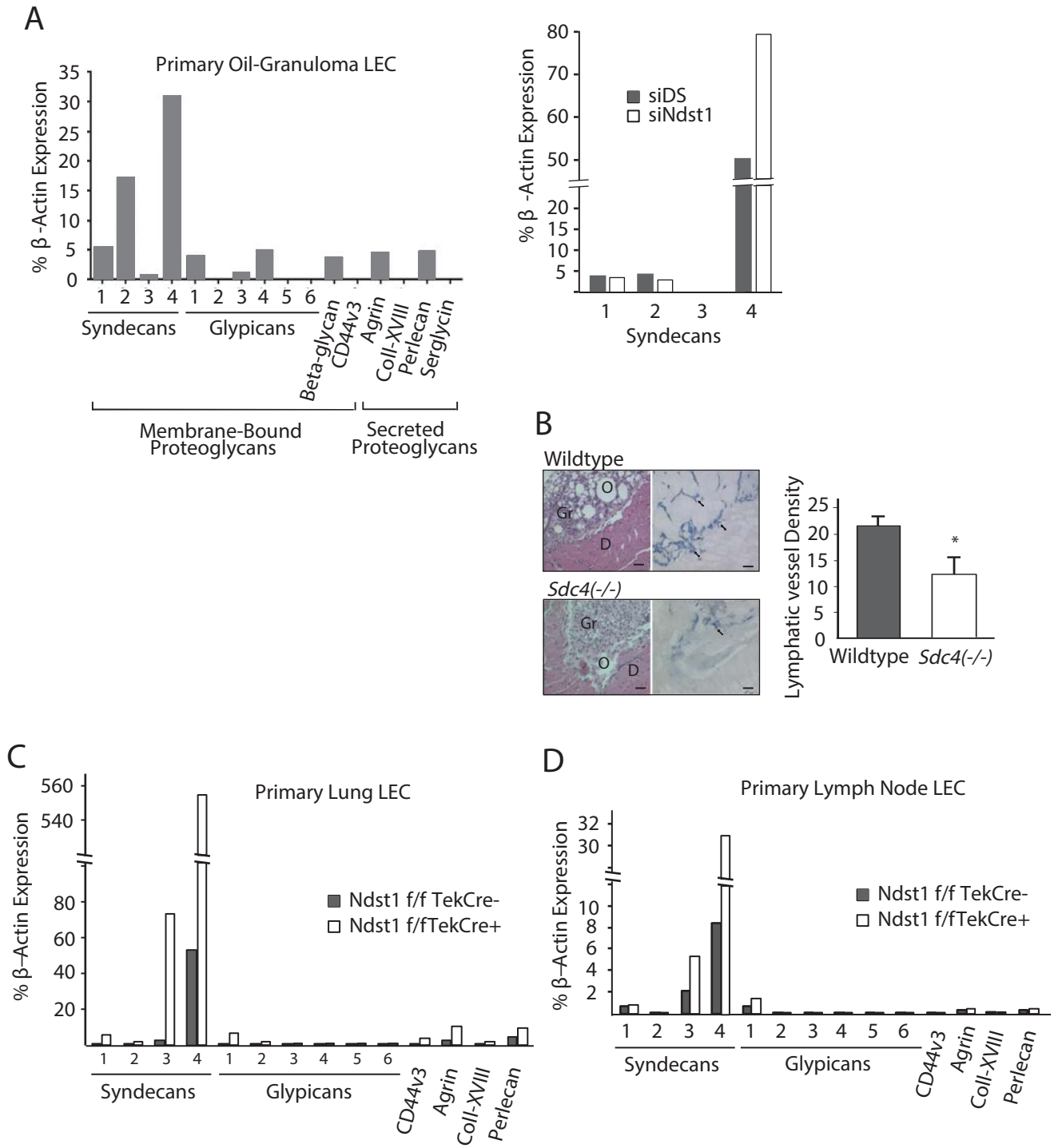


Figure 5

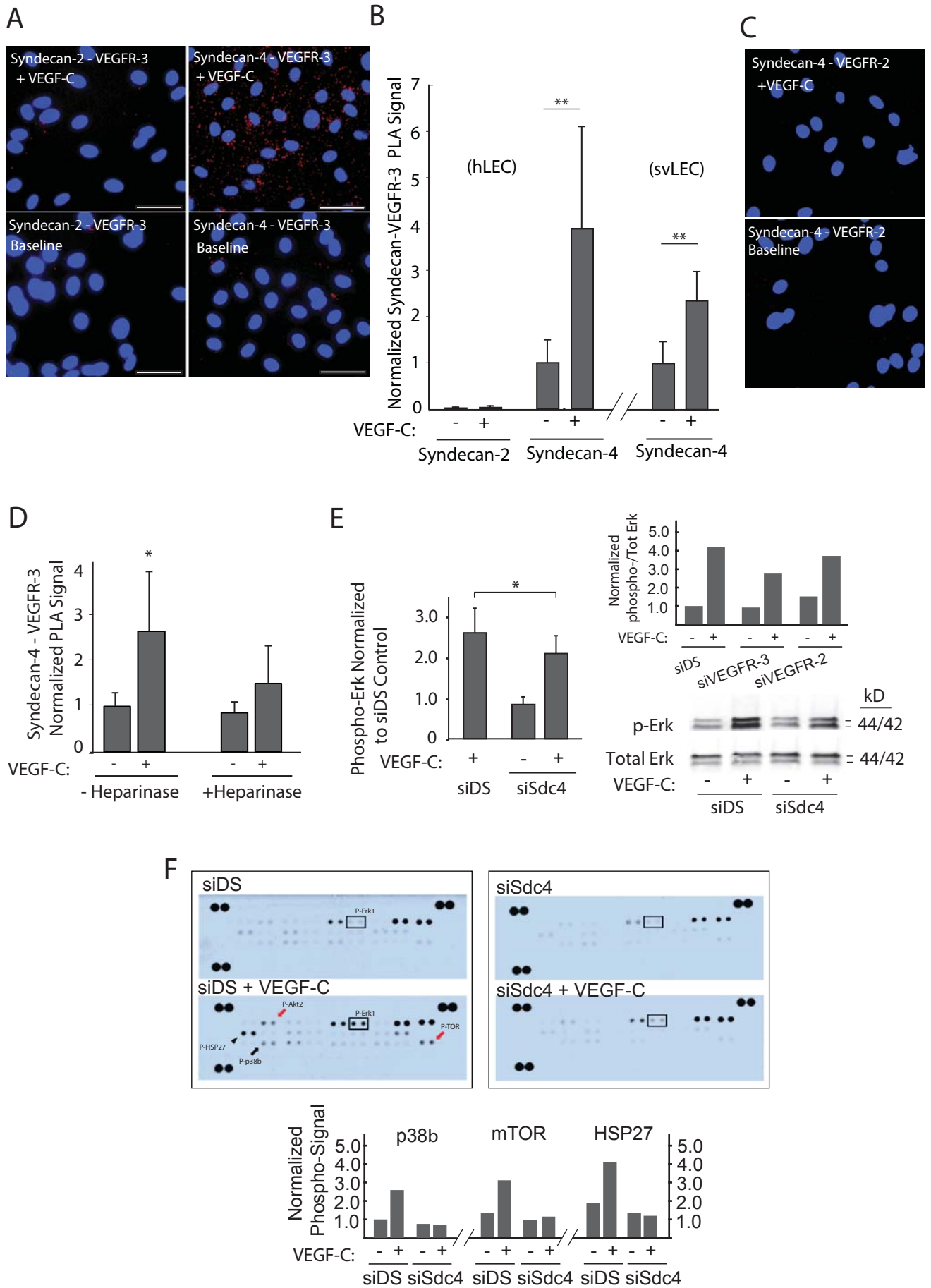
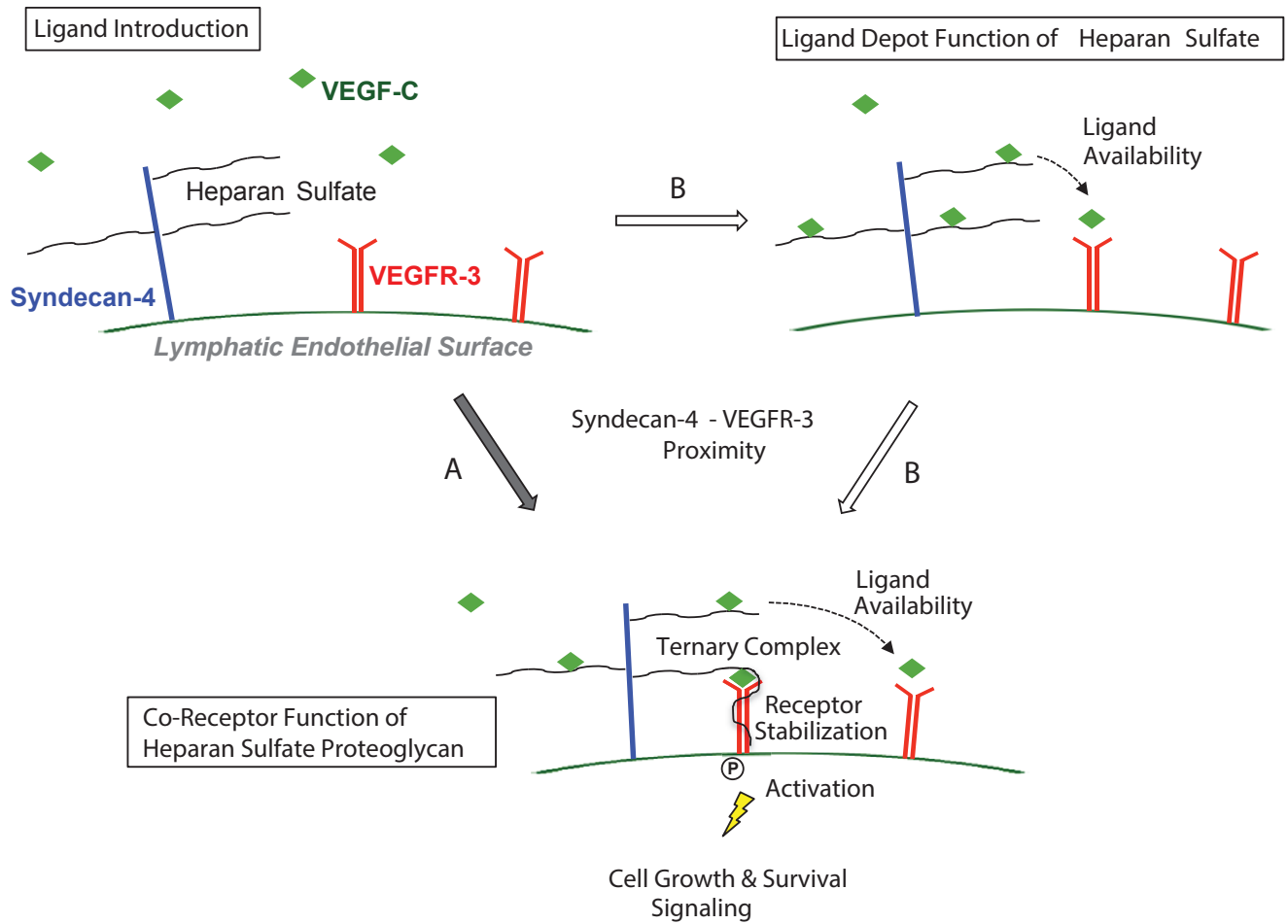


Figure 6



# Circulation Research

JOURNAL OF THE AMERICAN HEART ASSOCIATION



**Functional Importance of a Proteoglycan Co-Receptor in Pathologic Lymphangiogenesis**  
Scott C Johns, Xin Yin, Michael Jeltsch, Joseph R Bishop, Manuela Schuksz, Roland El Ghazal,  
Sarah A Wilcox-Adelman, Kari Alitalo and Mark M Fuster

*Circ Res.* published online May 25, 2016;  
*Circulation Research* is published by the American Heart Association, 7272 Greenville Avenue, Dallas, TX 75231  
Copyright © 2016 American Heart Association, Inc. All rights reserved.  
Print ISSN: 0009-7330. Online ISSN: 1524-4571

The online version of this article, along with updated information and services, is located on the  
World Wide Web at:

<http://circres.ahajournals.org/content/early/2016/05/25/CIRCRESAHA.116.308504>  
Free via Open Access

Data Supplement (unedited) at:

<http://circres.ahajournals.org/content/suppl/2016/05/25/CIRCRESAHA.116.308504.DC1.html>

**Permissions:** Requests for permissions to reproduce figures, tables, or portions of articles originally published in *Circulation Research* can be obtained via RightsLink, a service of the Copyright Clearance Center, not the Editorial Office. Once the online version of the published article for which permission is being requested is located, click Request Permissions in the middle column of the Web page under Services. Further information about this process is available in the [Permissions and Rights Question and Answer](#) document.

**Reprints:** Information about reprints can be found online at:  
<http://www.lww.com/reprints>

**Subscriptions:** Information about subscribing to *Circulation Research* is online at:  
<http://circres.ahajournals.org/subscriptions/>

## SUPPLEMENTAL MATERIAL

### DETAILED METHODS:

#### Mouse Genetic Models:

*Ndst1<sup>flf</sup>TekCre<sup>+</sup>* mutants were generated as described<sup>1</sup>. Syndecan-4 homozygous-null mice (*Sdc4<sup>-/-</sup>*)<sup>2</sup> (kindly provided by P. Goetinck, Massachusetts General Hospital) were used to generate oil-granuloma/lymphangioma lesions<sup>3</sup>. For some studies, lesions were examined in compound (*Sdc4<sup>-/-</sup>*)*Ndst1<sup>flf</sup>TekCre<sup>+</sup>* mutants (after crossing *Ndst1<sup>flf</sup>TekCre<sup>+</sup>* onto the *Sdc4<sup>-/-</sup>* background). For carcinoma models, transgenics expressing polyoma middle T-antigen (*PyMT*) under control of the mammary tumor virus (*MMTV*) promoter (*MMTV-PyMT*; Jackson) were backcrossed onto C57Bl/6. *MMTV-PyMT* heterozygosity was sufficient for development of palpable breast tumors in 12-week females. Compound male heterozygotes (*Ndst1<sup>flf</sup>TekCre<sup>+</sup>PyMT<sup>+/-</sup>*) were crossed with wildtype *Ndst1<sup>flf</sup>* females (which had been extensively backcrossed onto the C57Bl/6 background). Among *PyMT<sup>+/-</sup>* tumor-susceptible female offspring, this generated ~50% *Ndst1<sup>flf</sup>TekCre<sup>+</sup>* mutants. Mutant (*Ndst1<sup>flf</sup>TekCre<sup>+</sup>*) versus wildtype (*Ndst1<sup>flf</sup>TekCre<sup>-</sup>*) *MMTV-PyMT<sup>+/-</sup>* females were sacrificed at 12 weeks for tumor-pathologic studies. To generate *Ndst1<sup>flf</sup>Prox1<sup>+CreERT2</sup>* mutants and *Ndst1<sup>flf</sup>Prox1<sup>-CreERT2</sup>* controls, *Prox1<sup>+CreERT2</sup>* mice (provided generously by G. Oliver, Memphis, TN)<sup>4</sup> were bred to *Ndst1<sup>flf</sup>* mice after backcrossing onto C57Bl/6. Tamoxifen (Sigma; dissolved in corn oil) was injected intraperitoneally into *Prox1<sup>+CreERT2</sup>* mutants (and *Prox1<sup>-CreERT2</sup>* littermate-controls) daily (0.12 mg/g body weight) for 5d to induce *Cre*-recombinase. *Prox1<sup>+CreERT2</sup>* mice were bred to *Rosa26R* reporter mice to assess *Cre* localization. LLC tumors were generated by subcutaneous delivery of 5 x 10<sup>5</sup> LLCs in 100µL PBS into the inguinal skin-fold. Cells were either VEGF-C overexpressing (LLC-VC) or empty-vector control (LLC-ev) LLCs simultaneously injected into the opposite inguinal region of the same animals, injected 7d following the first tamoxifen dose. Tumors were isolated for pathologic analysis 10d after cell-injection. Mice were housed in AAALAC-approved vivaria following IACUC standards, maintained on a 12hr light-dark cycle, weaned at 3-4 weeks age, and fed standard chow *ad libitum*. For injections, animals were anesthetized using isoflurane (2.5%) through an oxygen-supplemented vaporizer system.

**Pathologic tissue processing and analysis:** Tumor/tissue specimens for some carcinoma and tissue-based were formalin-fixed, paraffin-embedded, and H&E stained. Sections were immunostained with rabbit-anti-mouse LYVE-1 (5µg/ml; Millipore) followed by biotin-conjugated anti-rabbit secondary (1µg/ml; Jackson), alkaline-phosphatase conjugated streptavidin (2µg/ml; Jackson), and Vector-Blue substrate (Vector). Endogenous peroxidases and avidin/biotin binding were blocked (Vector-kit), with proteinase-K used for antigen retrieval (Dako). Nuclear-Fast-Red counterstain was used. Mean lymphatic vessel density (LVD) was quantified as average number of lymphatic processes per high-power microscopic field. For each tumor, multiple fields were quantified from 2 macroscopically separated levels, with fields selected by a staff pathologist blinded to genotype. Images were photographed (Nikon Eclipse-80i; 40X objective at RT). Peroxidase-based TUNEL was used following manufacturer protocol (Roche). For VEGF-C staining, blocked sections were incubated in rabbit-anti-VEGF-C overnight (10µg/ml; Abcam, or rabbit-IgG control; 4°C) in blocking buffer; and treated with biotin anti-rabbit (1.5µg/ml; Vector) and streptavidin-Cy3 (1µg/ml; Jackson).

**Lymphangiogenesis assessments in tissue from LLC tumor bearing mice:** Formalin-fixed paraffin-embedded tumor sections were heat-denatured in citrate buffer, blocked (1%BSA/TTBS), treated with goat-anti-LYVE-1 (5 $\mu$ g/ml; R&D) and Cy3 anti-goat (2 $\mu$ g/ml; Abcam) antibodies, cover-slipped with Vectashield (Vector), and photographed (Nikon Eclipse-80i; 40X objective at RT). Lymphangiogenesis only occurred along the tumor periphery in this model: LVD was calculated as average number of vessels/field for all tandem high-power fields along the tumor-periphery (acquired and quantified blinded to genotype). In some studies, LLC-VC cells were injected intravenously (1x10<sup>5</sup> cells/mouse) post-tamoxifen to establish orthotopic lung-tumor foci. At 10d post-injection, mice were sacrificed, and lungs digested (0.2% type-I collagenase; Sigma), with washed suspensions subjected to immuno-labeling described separately.

**Neonate lymphatic whole-mount analyses:** For whole-mount analyses, ear tissue from sacrificed newborn mice within age 1-week was examined. Following fixation (4% paraformaldehyde), dermis was mechanically exposed, permeabilized with triton, and blocked overnight in 3% goat serum in labeling buffer (0.3% triton X-100/ PBS; 4°C). Rabbit anti-mouse LYVE-1 was applied overnight in labeling buffer (1 $\mu$ g/ml; Abcam; 4°C), followed overnight again by goat anti-rabbit Cy3 (1 $\mu$ g/ml; Abcam). Tissue was mounted (Vectashield), and fields (imaged with 10X objective; RT) were analyzed for lymphatic vessel density by the method of grid intersection<sup>5</sup>. Adobe CS2-photoshop software was used to quantify and analyze grid images (blinded to genotype). Lymphatic vessel density (grid-intersection) values for each genotype were calculated, with normalized values (+/-SD) plotted on corresponding graph. Values were compared with appropriate t-test statistic used to calculate p-value reported in corresponding Figure legend.

**Wound lymphangiogenesis:** was examined in the setting of an early wound-healing model<sup>6</sup> initiated through a standard 3mm cylindrical full-thickness punch biopsy on the dorsal skin of anesthetized mutant versus wildtype littermates. After four days, mice were sacrificed, and the entire wound from each mouse, including a margin of normal surrounding skin, was excised using a wide (8mm) cylinder biopsy. Samples were then split coronally with respect to the wound-crater center, with a piece from each transferred to paraffin embedding so as to allow microtome coronal-sections to be taken for histology. Paraffin sections treated with Hemo-De clearing agent (Fisher) were rehydrated. Antigen retrieval was performed through a 10 min Proteinase K incubation; and endogenous avidin and biotin were blocked. Samples were then blocked in 1%BSA/TTBS blocking buffer (1 hr at RT) followed by addition of goat anti-LYVE-1 (5 $\mu$ g/ml; R&D) and incubation overnight at 4°C. Samples were then incubated in Biotin anti-goat (20 $\mu$ g/ml; R&D) for 1 hr in blocking buffer, followed by streptavidin-AP (1 $\mu$ g/ml; Vector) for 1 hr at RT. Vector Blue (Vector Labs) substrate was added to slides and incubated for 15 min. Vectashield (Vector Labs) was added to the slides, and images were photographed (Nikon Eclipse 80i; 40X objective at RT). Lymphatic vessels in the column of adjacent high-power (40X objective) fields covering the wound border on each side of the wound crater (from epidermis to base of dermis) were quantified while blinded to genotype, and used to calculate the density or index of total lymphatic vessels per wound margin.

**Immunoblotting:** Serum-starved cells were stimulated with mature VEGF-C (100ng/mL, 15min for most studies). Cells were lysed in RIPA (50mM Tris (pH 7.4), 0.15M NaCl, 10mM MgCl<sub>2</sub>, 10mM CaCl<sub>2</sub>, 1mM EDTA, 1 $\mu$ l/ml protease inhibitors (Sigma), 1mM PMSF, 0.1% SDS, 1% Triton X-100, 1% sodium deoxycholate, and 1mM sodium orthovanadate), followed by freezing. Thawed samples were separated on 4-15% gradient gels with rabbit-polyclonal antibodies against phospho-(Ser<sup>473</sup>)Akt (1:1000; Cell Signaling), total-Akt, phospho-Erk1/2 (1:1000; Cell

Signaling), or total-Erk to probe membranes, followed by IRdye-conjugated anti-rabbit antibody (1:10000; LI-COR). Bands were normalized to the ratio of phospho-/Total Akt for baseline-starved cells on a Odyssey/LI-COR infrared system. For cleaved-caspase-3 studies, to examine the effect of VEGF-C on apoptotic signaling in cultured serum-starved siRNA treated hLECs, hLECs were starved for 6hr in the presence/absence of 1 $\mu$ g/mL mature VEGF-C, lysed in RIPA; and run on 4-15% gradient gels (BioRad). In some cases during pilot studies, starvation was varied to include other non-VEGF-C growth factors +/- serum in the basal medium. Blots were labeled with rabbit-anti-caspase (1:1000; Cell Signaling) or cleaved-caspase-3 (1:500; Cell Signaling) antibodies. Bands were quantified following anti-rabbit IRdye labeling.

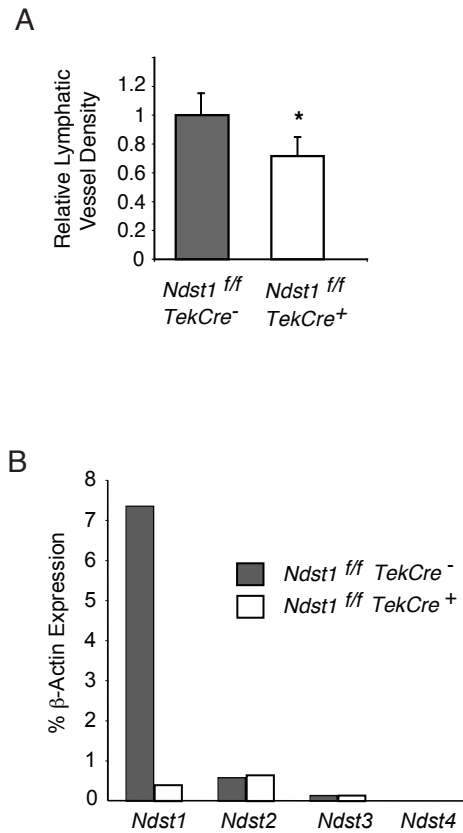
**Phospho-MAPK Array:** For array studies, human lung lymphatic primary endothelial cells (hLEC) were grown to 70-80% confluency in a 60mm dishes. Cells were transfected with 20nM of siRNA using Lipofectamine RNAiMAX (ThermoFisher) following manufacturer recommendations. Briefly, cells were rinsed with PBS, and transfection complex was added in Opti-Mem (ThermoFisher) and incubated for 6 hours. The cells were rinsed with PBS and normal growth media was added, followed by overnight recovery. Cells were then serum starved for a total of 5 hours in DMEM with a 30 min media change at the end of starvation. Human recombinant VEGF-C (R&D Systems) was then added at 100ng/mL and incubated for 15 min. Cells were then lysed in 0.5mL NP-40 lysis buffer. Using starved (baseline) versus post-VEGF-C stimulation lysates, the array was completed following manufacturer instructions (R&D). Reference dots (on 3 slide-corners) confirmed for each slide that streptavidin-HRP had been appropriately incubated during the procedure.

**Proteoglycan core-protein blotting:** Cultured near-confluent hLEC pre-treated +/- heparinase to destroy heparan sulfate chains were lysed, electrophoresed on SDS-PAGE, and examined for HSPG core proteins by probing blots with an antibody directed against HS "stubs" (anti- $\Delta$ HS). The latter remain on HSPG core proteins as neo-epitopes, consisting of the non-reducing (glucuronate) glycan termini generated by digestion of cell-surface HSPGs with heparinase, with methodology as published<sup>7</sup>. Lysates were run on a 4-15% SDS-PAGE gel, transferred, and blotted with mouse anti- $\Delta$ HS antibody (1:1000 overnight at 4°C; clone 3G10, a kind gift from Dr G. David) which recognizes the stub neo-epitopes on HSPG core proteins. After incubation in IRdye 680-conjugated anti-mouse antibody (1:10,000; LI-COR), blots were visualized/photographed using a Odyssey/LI-COR infrared system. In a separate blot using the same SDS PAGE-gel and reagents, instead of treating with 3G10 antibody, the lysate from heparinase-treated cells was incubated solely with rabbit anti-human syndecan-4 antibody (1:1000, Abcam), and examined in the LI-COR system after incubation with anti-rabbit IRdye 800 (1:10,000; LI-COR).

#### SUPPLEMENTAL REFERENCES:

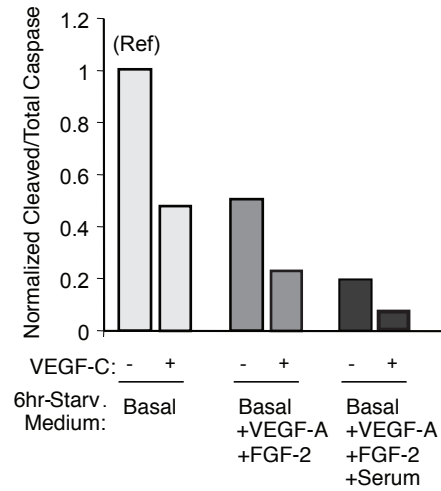
1. Wang L, Fuster M, Sriramarao P and Esko JD. Endothelial heparan sulfate deficiency impairs L-selectin- and chemokine-mediated neutrophil trafficking during inflammatory responses. *Nat Immunol.* 2005;6:902-10.
2. Echtermeyer F, Streit M, Wilcox-Adelman S, Saoncella S, Denhez F, Detmar M and Goetinck P. Delayed wound repair and impaired angiogenesis in mice lacking syndecan-4. *J Clin Invest.* 2001;107:R9-R14.
3. Mancardi S, Stanta G, Dusetti N, Bestagno M, Jussila L, Zweyer M, Lunazzi G, Dumont D, Alitalo K and Burrone OR. Lymphatic endothelial tumors induced by intraperitoneal injection of incomplete Freund's adjuvant. *Exp Cell Res.* 1999;246:368-75.

4. Srinivasan RS, Dillard ME, Lagutin OV, Lin FJ, Tsai S, Tsai MJ, Samokhvalov IM and Oliver G. Lineage tracing demonstrates the venous origin of the mammalian lymphatic vasculature. *Genes Dev.* 2007;21:2422-32.
5. Kirchner LM, Schmidt SP and Gruber BS. Quantitation of angiogenesis in the chick chorioallantoic membrane model using fractal analysis. *Microvasc Res.* 1996;51:2-14.
6. Fuster MM, Wang L, Castagnola J, Sikora L, Reddi K, Lee PH, Radek KA, Schuksz M, Bishop JR, Gallo RL, Sriramarao P and Esko JD. Genetic alteration of endothelial heparan sulfate selectively inhibits tumor angiogenesis. *J Cell Biol.* 2007;177:539-49.
7. Govindraj P, West L, Koob TJ, Neame P, Doege K and Hassell JR. Isolation and identification of the major heparan sulfate proteoglycans in the developing bovine rib growth plate. *J Biol Chem.* 2002;277:19461-9.

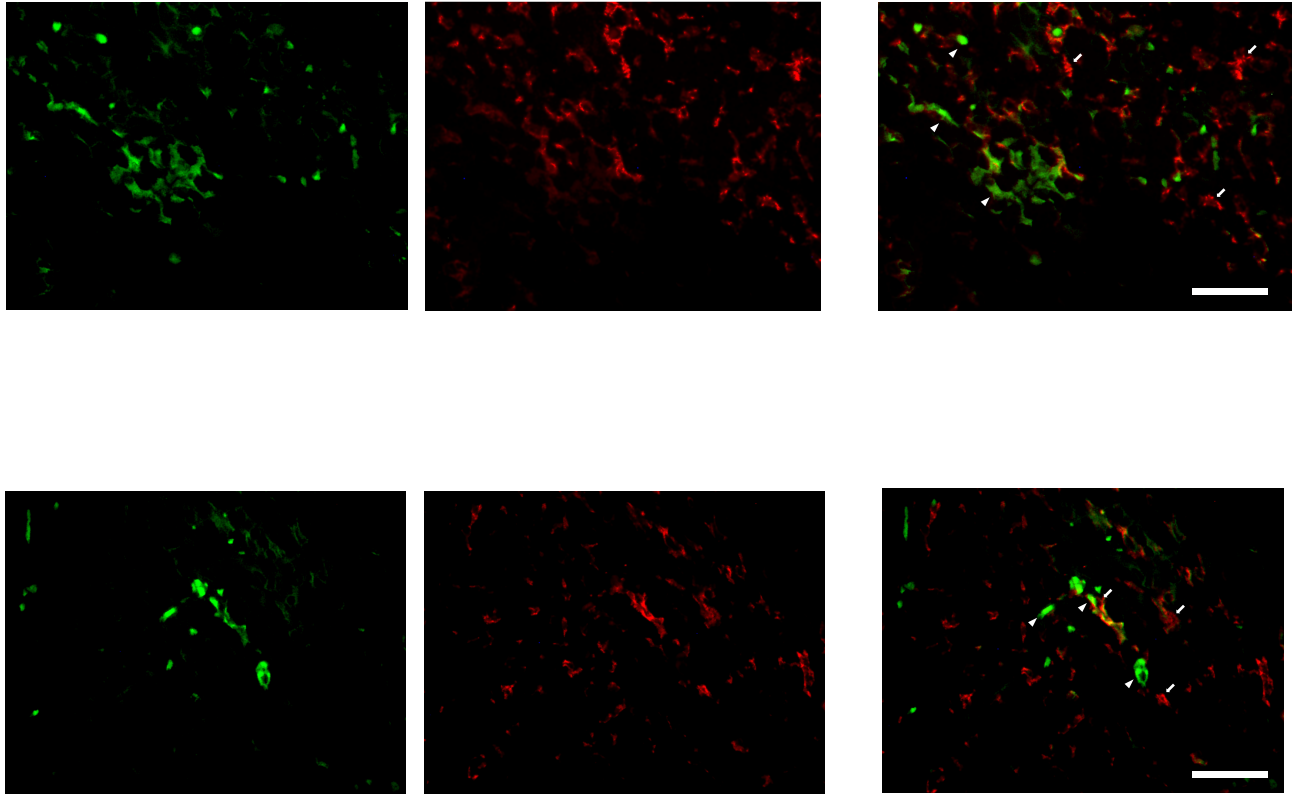


**Online Figure I. Neonatal ear-bud lymphangiogenesis in *Ndst1*<sup>f/f</sup>*TekCre*<sup>+</sup> mutant mice and their *Cre*- littermates.**

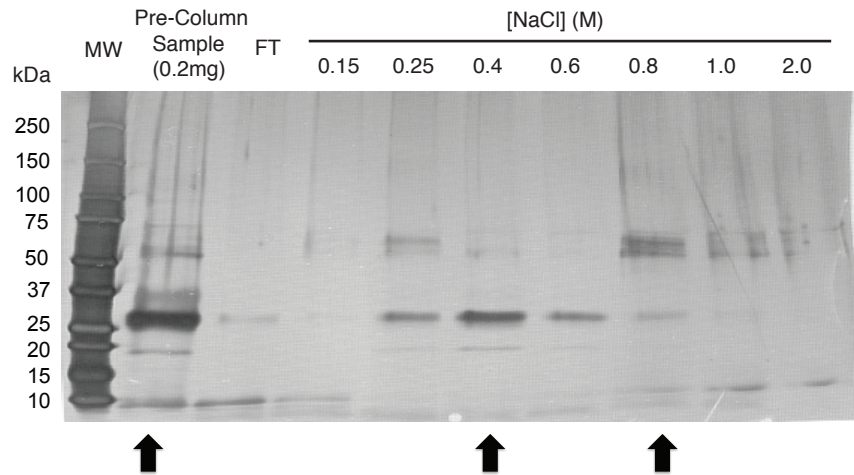
(A) To examine early developing lymphatic trunks/ vasculature in dermis of the neonatal ear-bud, whole-mount sections were stained for LYVE-1 (from n=10 *Ndst1*<sup>f/f</sup>*TekCre*<sup>+</sup> mutants versus n=7 *Cre*- wildtype littermates; \*P<0.001 for difference in lymphatic vessel density). (B) To assess deletion efficiency of the mutation in lymphatic vasculature, primary lymphatic endothelial cells purified from the lungs of either *Ndst1*<sup>f/f</sup>*TekCre*<sup>+</sup> mutant mice or their *Cre*- littermates were examined for the expression of major heparan sulfate proteoglycan core proteins using quantitative PCR. RNA was isolated, reverse transcribed, amplified using gene specific primers to each proteoglycan core protein, and quantified relative to expression of  $\beta$ -actin. Ct values from duplicate assays were used to calculate % expression.



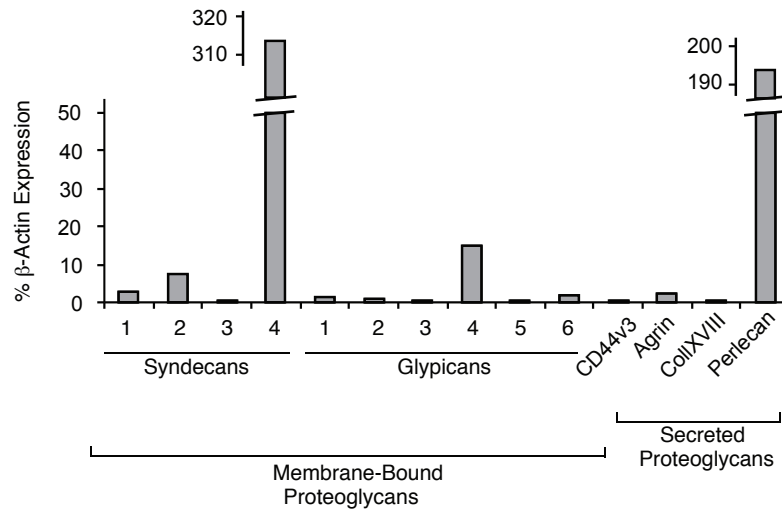
**Online Figure II. VEGF-C mediated protection from apoptotic stress in primary human lung lymphatic endothelial cells.** Cultured primary human lymphatic endothelial cells (hLEC) grown in fully supplemented medium (including VEGF-A, FGF-2, and 5% serum) were tested for the ability of human recombinant VEGF-C to protect from apoptosis following exposure to a variety of media conditions over a 6 hour period, including full starvation (“Basal” medium) and additional supplementation, as indicated on the left graph. Measurements are based on the ratio of cleaved- to total caspase-3, as measured by Western blotting (with densitometry normalized to the value for fully-starved untreated cells).



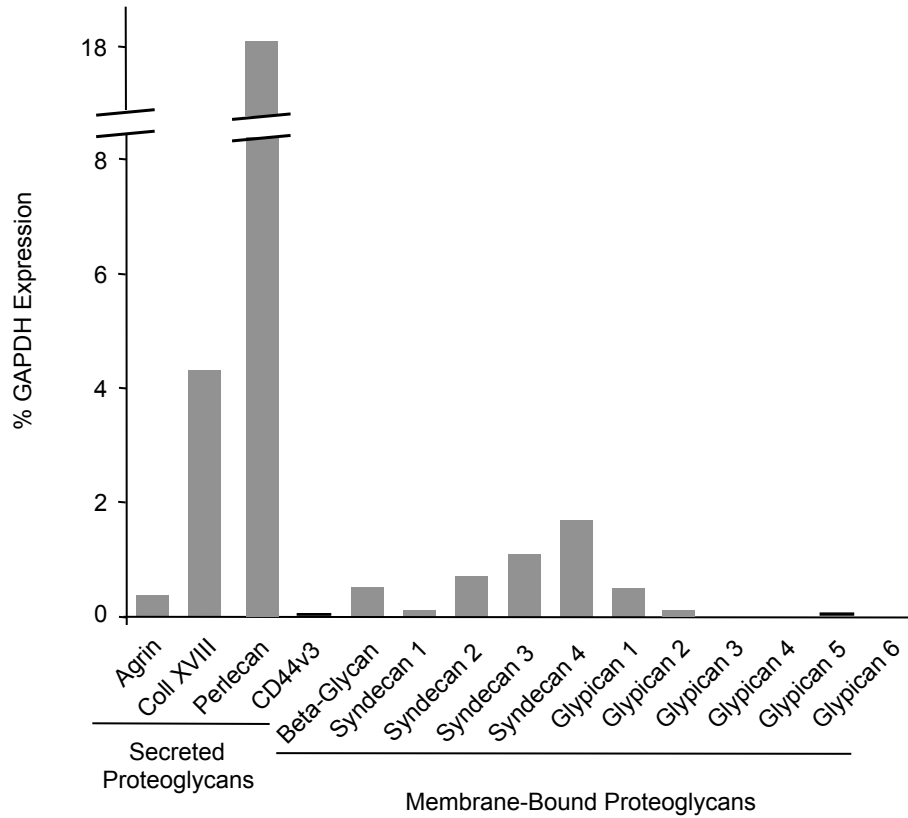
**Online Figure III. LYVE-1 and F4/80 labeling in periphery of LLC-VC tumors.** Sections from VEGF-C over-expressing tumors (as used for tumor analysis in Figure 2) were labeled with anti-mouse LYVE-1 (green) and F4/80 (red) antibodies, and photomicrographs were taken using a 40X objective, with merge images to right. Representative images are shown for periphery of such tumors (wherein lymphangiogenesis was quantified using LYVE-1 analysis in Fig.2); demonstrating essentially independent LYVE-1 structures bordered (occasionally in close-proximity) with F4/80+ macrophages. (Bar = 50  $\mu$ m).



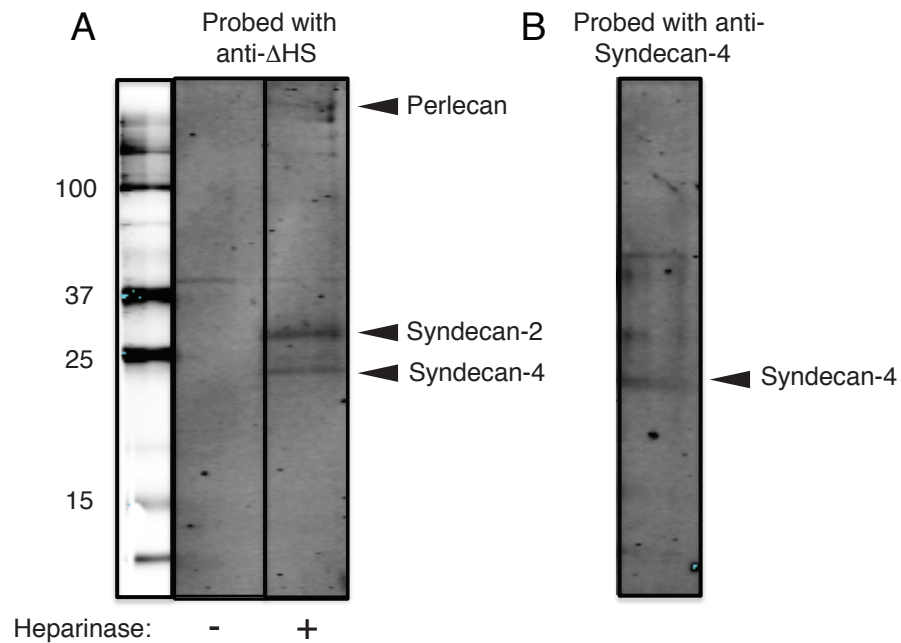
**Online Figure IV. Heparin Sepharose Affinity Chromatography: Pro-VEGF-C Binding Profile.** To assess binding of Pro-VEGF-C to commercial heparin, and to assess the molecular weight of NaCl-eluted species, affinity chromatography using heparin sepharose columns was carried out, and elutions were silver stained through standard methodology. Fractions collected over the indicated NaCl step-concentration range were run on SDS-PAGE with silver staining to reveal the protein elution profile. The level to which native protein migrates on the gel is shown at left (“Pre-column” sample in lane 1 with kD ladder indicated to the left); column flow-through “FT” is shown in lane 2; and elution profile (subsequent lanes) is shown to the right. This preparation of “Pro-VEGF-C” produced in CHO cells (see “Methods” section) is actually a mixture composed of multiple species/bands noted in the pre-column sample (left arrow at bottom of blot), with a predominant (partially-processed) pro-peptide VEGF-C species that elutes in the 0.4M – 0.5M NaCl range (29/31kD major band; middle arrow), a much lesser amount of the most proteolytically processed mature form of VEGF-C (~18kD band), and an additional band of “full-length” unprocessed VEGF-C that mostly elutes in the 0.8M range (58kD band; right arrow).



**Online Figure V. Expression of major heparan sulfate proteoglycan core proteins in SV-LEC line of lymphatic endothelial cells.** Mouse SV-LEC cells, a SV40 Large T-antigen immortalized lymphatic endothelial cell line derived from mouse mesenteric lymphatic endothelia, were examined for the expression of major heparan sulfate proteoglycan core proteins using quantitative PCR. RNA was isolated, reverse transcribed, amplified using gene specific primers to each proteoglycan core protein, and quantified relative to expression of  $\beta$ -actin. Ct values from triplicate assays were used to calculate % expression. Bars and scale are interrupted to indicate that values for syndecan-4 and perlecan expression in this cell-line were approximately three-fold (314%) and two-fold (197%) that of beta-actin expression, respectively.



**Online Figure VI. Expression of major heparan sulfate proteoglycan core proteins in primary human dermal microvascular endothelial cells (HDMEC).** Cultured commercial HDMECs were examined for the expression of major heparan sulfate proteoglycan core proteins using quantitative PCR. RNA was isolated, reverse transcribed, amplified using gene specific primers to each proteoglycan core protein, and quantified relative to expression of GAPDH. Ct values from triplicate assays were used to calculate % expression. Bar and scale is interrupted to plot dominant expression of the secreted HSPG perlecan in these cells, while illustrating expression pattern for membrane-bound syndecans.



**Online Figure VII. Assessment of HSPG core proteins produced by primary human lymphatic endothelial cells (hLEC).** Cultured near-confluent hLEC pre-treated +/- heparinase were lysed, electrophoresed on SDS-PAGE, and examined for HSPG core proteins by probing blots with an antibody directed against HS "stubs" (anti- $\Delta$ HS). The latter remain on any HSPG core protein as neo-epitopes after heparinase digestion, with methodology as published<sup>5</sup>. (A) Lysate from heparinase-treated cells (right lane, labeled "+" at bottom) reveals multiple bands, including two dominant bands in the 20-40kD range at molecular weights characteristic for syndecan-4 (lower band, labeled) and syndecan-2 immediately above it. The heaviest band at top of blot is consistent with the secreted HSPG perlecan (also labeled). Lysate from non-heparinase treated cells (labeled "-" at bottom) served as a negative control. (B) Blot from a separate SDS-PAGE gel that was run in parallel on lysate from heparinase-treated cells, and probed for syndecan-4 (labeled) using an anti-syndecan-4 antibody. Upper thin band on the blot (unlabeled) was also noted to be present in both heparinase and non-heparinase lysates on panel (A), and thus appeared to be nonspecific.

## Online Table I

Primer Sequences (Forward/ Reverse) used for Quantitative PCR of major mouse HS core proteins.

HS Core Protein:	Forward Primer:	Reverse Primer:
Syndecan1	GGAGCAGGACTTCACCTTTG	TACAGCATGAAACCCACCAG
Syndecan2	GCTGCTCCAAAAGTGGAAAC	CAGCAATGACAGCTGCTAGG
Syndecan3	GAGCCTGACATCCCTGAGAG	CCCACAGCTACCACCTCATT
Syndecan4	GAGCCCTACCAGACGATGAG	CAGTGCTGGACATTGACACC
Glypican1	AGCGAGATGGAGGAGAACCT	CTGAGTACAGGTCCCAGGAA
Glypican2	TGACTACCTGCTCTGCCTCTC	GCTTCGCTGACCACATTCT
Glypican3	GGCAAGTTATGTGCCCATTC	ATGTAGCCAGGCAAAGCACT
Glypican4	ATGGTGGCAGAGAGGCTAGA	GGAACGAGAAATTCGTCCAG
Glypican5	AAGCCCAGTCTGGAAATCCT	TCACAGTCCCCACTGACTTG
Glypican6	CACGTTTCAGGCCCTACAAT	GTTCCAGCATTCTCCTCGT
Agrin	AACCTGGAGGAGGTGGAGTT	CTTCTTGCAGACGCAGGAC
Perlecan	CACTCGCTCCATCGAGTACA	GATGACCCTGAGCAGCATCT
Collagen-XVIII	CTGGGAGGCTCTGTTCTCAG	CACAGTAGCTCTCGGTCAGC
Beta-glycan	TGAAGTGACTGGACGAGACG	AGTGCGGAGATTCAGGACAT
CD44v3	CTGGGAGCCAAATGAAGAAA	AGCACTTCCGGATTTGAATG
Serglycin	GAGCACCCCTGCTACATTTCC	CCGCGTAGGATAACCTTGAA